Article

Functional genomic landscape of cancer-intrinsic evasion of killing by T cells

https://doi.org/10.1038/s41586-020-2746-2

Received: 9 September 2019

Accepted: 30 June 2020

Published online: 23 September 2020

Check for updates

Keith A. Lawson[1,2,3,12], Cristovão M. Sousa[4,12], Xiaoyu Zhang[1,2], Eiru Kim[5,6], Rummy Akthar[1,2], Joseph J. Caumanns[1], Yuxi Yao[1,2], Nicholas Mikolajewicz[1], Catherine Ross[1], Kevin R. Brown[1], Abdelrahman Abou Zid[1,7], Zi Peng Fan[4], Shirley Hui[1], Jordan A. Krall[4], Donald M. Simons[4], Chloe J. Slater[4], Victor De Jesus[4], Lujia Tang[4], Richa Singh[4], Joshua E. Goldford[4], Sarah Martin[4], Qian Huang[1], Elizabeth A. Francis[1], Andrea Habsid[1], Ryan Climie[1], David Tieu[1], Jiarun Wei[1], Ren Li[8], Amy Hin Yan Tong[1], Michael Aregger[1], Katherine S. Chan[1], Hong Han[1], Xiaowei Wang[1], Patricia Mero[1], John H. Brumell[2,8], Antonio Finelli[3], Laurie Ailles[9,10], Gary Bader[1,2], Gromoslaw A. Smolen[4,11], Gillian A. Kingsbury[4], Traver Hart[5,6], Charles Kung[4] & Jason Moffat[1,2,7]✉

The genetic circuits that allow cancer cells to evade destruction by the host immune system remain poorly understood[1–3]. Here, to identify a phenotypically robust core set of genes and pathways that enable cancer cells to evade killing mediated by cytotoxic T lymphocytes (CTLs), we performed genome-wide CRISPR screens across a panel of genetically diverse mouse cancer cell lines that were cultured in the presence of CTLs. We identify a core set of 182 genes across these mouse cancer models, the individual perturbation of which increases either the sensitivity or the resistance of cancer cells to CTL-mediated toxicity. Systematic exploration of our dataset using genetic co-similarity reveals the hierarchical and coordinated manner in which genes and pathways act in cancer cells to orchestrate their evasion of CTLs, and shows that discrete functional modules that control the interferon response and tumour necrosis factor (TNF)-induced cytotoxicity are dominant sub-phenotypes. Our data establish a central role for genes that were previously identified as negative regulators of the type-II interferon response (for example, *Ptpn2*, *Socs1* and *Adar1*) in mediating CTL evasion, and show that the lipid-droplet-related gene *Fitm2* is required for maintaining cell fitness after exposure to interferon-γ (IFNγ). In addition, we identify the autophagy pathway as a conserved mediator of the evasion of CTLs by cancer cells, and show that this pathway is required to resist cytotoxicity induced by the cytokines IFNγ and TNF. Through the mapping of cytokine- and CTL-based genetic interactions, together with in vivo CRISPR screens, we show how the pleiotropic effects of autophagy control cancer-cell-intrinsic evasion of killing by CTLs and we highlight the importance of these effects within the tumour microenvironment. Collectively, these data expand our knowledge of the genetic circuits that are involved in the evasion of the immune system by cancer cells, and highlight genetic interactions that contribute to phenotypes associated with escape from killing by CTLs.

Cancer cells must acquire phenotypic changes that allow them to evade recognition and destruction by effector cells of the immune system such as CTLs. These phenotypic changes not only facilitate the progressive expansion and dissemination of cancer cells during tumorigenesis, but also promote resistance to immunotherapies that harness the potent cytotoxic properties of CTLs, including checkpoint inhibitors and chimaeric antigen receptor T (CAR-T) cells. Previous genomic studies of patients with cancer who were treated with immunotherapy have provided fundamental insights into several mechanisms that promote immune evasion (for example, loss of antigen presentation machinery or defects in interferon signalling)[4–6], but these studies are limited to the detection of frequently occurring genetic alterations. More recently, functional genomic screens using CRISPR–Cas9 approaches have shed light on the mechanistic basis of cancer-intrinsic CTL evasion[7–11].

[1]Donnelly Centre, University of Toronto, Toronto, Ontario, Canada. [2]Department of Molecular Genetics, University of Toronto, Toronto, Ontario, Canada. [3]Division of Urology, Department of Surgery, Princess Margaret Cancer Centre, University Health Network, Toronto, Ontario, Canada. [4]Agios Pharmaceuticals, Cambridge, MA, USA. [5]Department of Bioinformatics and Computational Biology, The University of Texas MD Anderson Cancer Center, Houston, TX, USA. [6]Department of Cancer Biology, The University of Texas MD Anderson Cancer Center, Houston, TX, USA. [7]Institute for Biomaterials and Biomedical Engineering, University of Toronto, Toronto, Ontario, Canada. [8]Cell Biology Program, The Hospital for Sick Children, Toronto, Ontario, Canada. [9]Department of Medical Biophysics, University of Toronto, Toronto, Ontario, Canada. [10]Ontario Institute for Cancer Research, Toronto, Ontario, Canada. [11]Present address: Celsius Therapeutics, Cambridge, MA, USA. [12]These authors contributed equally: Keith A. Lawson, Cristovão M. Sousa. ✉e-mail: j.moffat@utoronto.ca

However, there remains a lack of data systematically cataloguing the genetic elements of cancer cells that act in a genotype-to-phenotype fashion to facilitate cancer-intrinsic CTL evasion.

Mapping genetic determinants of CTL evasion

To build a platform for genome-wide phenotypic screens in mouse cancer cell lines for the systematic identification of genes associated with cancer-intrinsic immune evasion, we first constructed, using empirically defined rules[12], an optimized *Streptococcus pyogenes* Cas9 (spCas9) guide RNA (gRNA) library containing 94,528 gRNAs that target 19,069 protein-coding genes. We then used this library (which we call the mouse Toronto KnockOut, or mTKO, library; Supplementary Table 1) to identify: (1) fitness genes required for the proliferation of mouse cancer cells; and (2) cancer-cell-intrinsic CTL-evasion genes. This was accomplished by performing pooled loss-of-function genetic screens across a panel of six engineered mouse cancer cell lines that express either haemagglutinin (HA) or ovalbumin (Ova) as marker antigens (Fig. 1a). For all screens, CRISPR-mutagenized cells were propagated in the presence or absence of preactivated antigen-specific CTLs to apply a selection pressure, with representative cell populations serially sampled at different time points and subjected to deep sequencing to identify gRNAs that were enriched or depleted relative to untreated cell populations (Fig. 1b, Supplementary Table 2; see Methods). The functional genomic diversity of our panel of cell lines, as well as the quality of the screens using the mTKO library, was confirmed by the analysis and refinement of reference essential and non-essential gene sets as previously described[12–17] (Extended Data Fig. 1, Supplementary Tables 3–6; see Supplementary Information).

To explore the genetic landscape of cancer-intrinsic CTL evasion, we interrogated our dataset to identify genes with differential fitness effects in CTL-treated versus control populations of cancer cells using the drugZ algorithm[18] (Fig. 1c, Extended Data Fig. 2a, Supplementary Table 7). This analysis revealed that more than 2,000 genes affect cancer cell fitness under CTL killing pressure in at least one of the six cell lines, with a mean of around 330 genes per screen (Extended Data Fig. 2b; false discovery rate (FDR) < 5%). Our identified genes included well-characterized cancer-intrinsic CTL-evasion genes that are frequently mutated in patients resistant to checkpoint immunotherapy (for example, *B2m*, *Jak1*, *Jak2*, *Ifngr1*, *Ifngr2*)[4,6] (Extended Data Fig. 2c). To further validate our dataset, we performed gene set enrichment analysis (GSEA), and observed the enrichment of well-characterized immune regulatory pathways: gRNAs that target genes involved in antigen presentation, Jak–Stat signalling and the interferon pathways mediated resistance to CTL killing, whereas those that target genes involved in necroptosis, p38 mitogen-activated protein kinase (MAPK) signalling and the NF-κβ pathway conferred sensitivity to CTLs[4,6–11] (Extended Data Fig. 2d, Supplementary Table 8). GSEA also highlighted pathways with previously underappreciated roles in regulating the responses of cancer cells to CTL-mediated killing, including resistor genes in nitric oxide production and mitochondrial metabolism (mitochondrial translation, electron transport chain), and sensitizer genes in glycosylphosphatidylinositol (GPI) anchor metabolism, endosomal trafficking, transcriptional regulation and autophagy (Extended Data Fig. 2d).

To identify gene networks that regulate cancer-intrinsic immune evasion, we performed a genetic co-similarity analysis and identified gene pairs that showed correlated drugZ profiles across our six CTL killing screens, using data from two time points (mid and end) (Supplementary Table 9). Only genes that were significant in at least three measurements (FDR < 5%, resistor or sensitizer) were included, as this maximized the co-annotation of genes to the same pathway (log-likelihood score of around 2; see Methods) while maintaining sufficient genome coverage (around 2.5%) (Extended Data Fig. 2e, f). The resulting network contained a total of 548 genes (Fig. 1d). High-ranking correlated gene pairs were more than tenfold enriched for co-annotation in KEGG pathways and 50-fold enriched in CORUM complexes relative to random gene pairs, demonstrating the ability of our network to capture functional modules that affect cancer-intrinsic CTL evasion (Extended Data Fig. 2g, h). Unsupervised clustering of the matrix revealed a modular structure in keeping with this functional coherence, with gene pairs within clusters being enriched for shared pathway annotations relative to the overall network (Extended Data Fig. 2i). Notably, this allowed us to identify functional modules of pathways that are known to act in a coordinated manner to regulate immune signalling (for example, mammalian target of rapamycin (mTOR) signalling, major histocompatibility complex (MHC) presentation, interferon response)—similar to what has been observed in large-scale networks of genetic interactions in model organisms[19,20] (Fig. 1d, Extended Data Fig. 2j). Our network therefore provides an initial glimpse of the genetic wiring that is involved in the evasion of CTLs by cancer cells.

Core cancer-intrinsic CTL-evasion genes

The substantial genetic and functional heterogeneity of cancers means that it is essential to identify phenotypically robust genetic regulators of immune evasion for the discovery and validation of drug targets[21]. We therefore adapted the Daisy model of gene essentiality to identify 'core cancer-intrinsic CTL-evasion genes' (Fig. 1e), which we defined simply as a sensitizer or a resistor gene that was present across three or more of the six cell lines that we screened (FDR < 5%). This analysis yielded 182 genes (Fig. 1f, Supplementary Table 10) that represent the major pathways identified in our global pathway analysis described above (Fig. 1g, Extended Data Fig. 2d). To validate this set of 182 genes, we cloned a mini-library of 1,664 gRNAs that target 367 genes—including all 182 of the core cancer-intrinsic CTL-evasion genes—and performed secondary CTL killing screens across the same six cell lines (Extended Data Fig. 3a, Supplementary Tables 11, 12). Relative to a tailored list of gene-targeting control gRNAs ($n = 728$), our validation screens revealed robust classification of a-priori-determined sensitizer and resistor gene perturbations for each cell line (Extended Data Fig. 3a, $P < 0.05$, Supplementary Tables 11, 12). Only 18 core cancer-intrinsic CTL-evasion genes were also required for cell proliferation under standard growth conditions (that is, core fitness genes) (Extended Data Fig. 3b).

We next used data from The Cancer Genome Atlas (TCGA) to examine associations between the core cancer-intrinsic CTL-evasion genes and established markers of effective anti-tumour T cell responses[4,5,22,23] (Extended Data Fig. 3c, Supplementary Table 13). Notably, compared to random gene sets, we detected significant positive correlations between the core CTL-evasion genes and IFNγ response ($P = 5.05 \times 10^{-8}$), leukocyte fraction ($P = 5.56 \times 10^{-6}$) and innate anti-PD-1 resistance ($P = 1.74 \times 10^{-3}$). Moreover, significant positive correlations were observed within the core CTL suppressor class for tumour lymphocyte infiltration ($P = 4.16 \times 10^{-4}$), cytolytic index ($P = 1.73 \times 10^{-4}$), lymphocytes ($P = 8.37 \times 10^{-4}$) and $CD8^+$ T cell fraction ($P = 2.61 \times 10^{-3}$) (Extended Data Fig. 3c–g). These data further highlight the importance of our functionally defined core CTL-evasion gene set, and directly link our observations in mouse cancer models to data from patients with cancer.

Resistance to IFNγ regulates CTL evasion

We ordered the core genes by computing the geometric mean rank across all screens, to highlight conserved hits with the strongest phenotypic effects across our dataset (Extended Data Fig. 3h, Supplementary Table 14). In addition to canonical upstream IFNγ signalling components (for example, *Ifngr1* and *Ifngr2*, *Jak1* and *Jak2*, *Stat1* and *Stat2*), these hits also included three negative regulators of IFNγ signalling—*Socs1*, *Ptpn2* and *Adar*[24,25]—that were identified as strong synthetic lethal hits with checkpoint immunotherapy in in vivo CRISPR screens performed in B16 melanoma cells[8,26]. Our data also show that

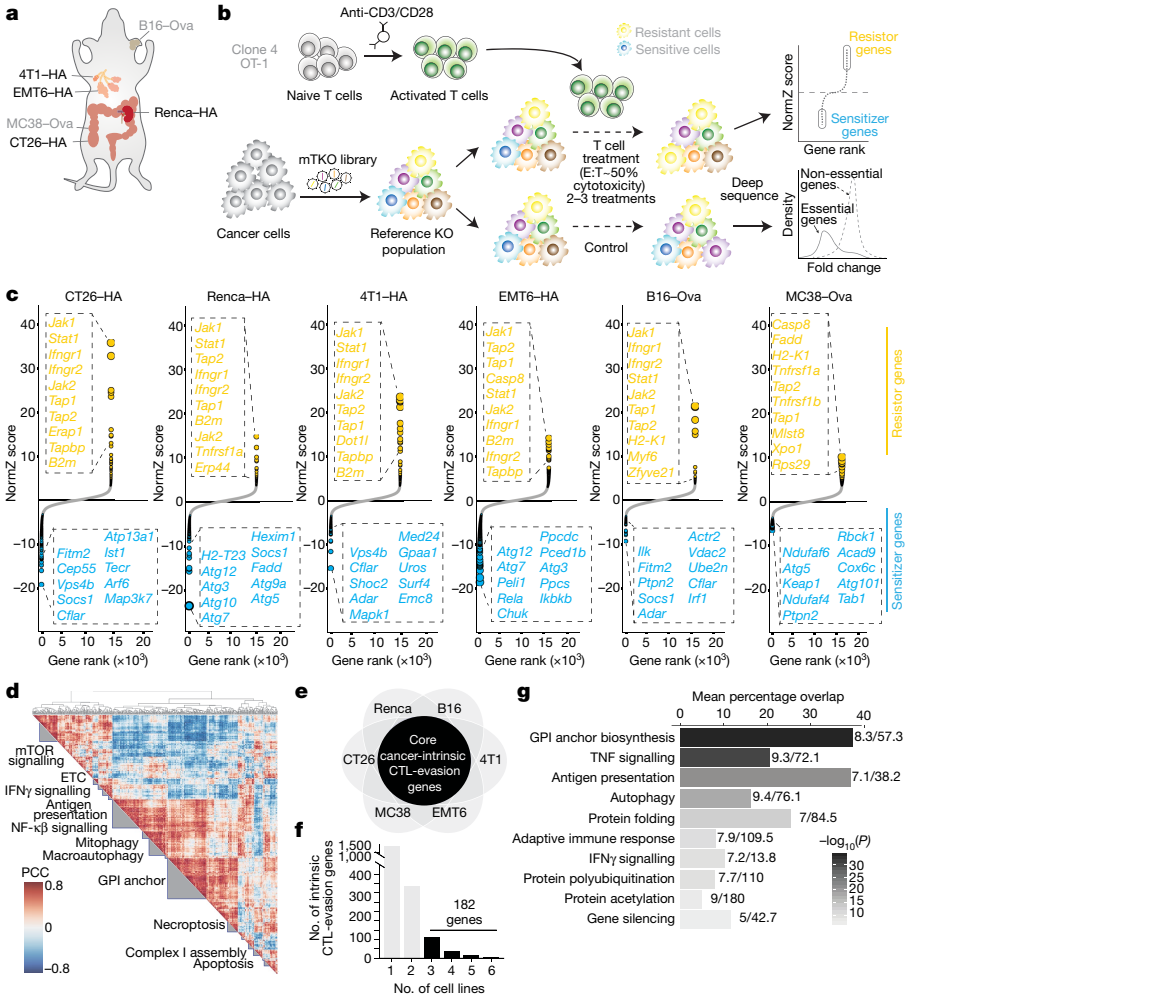

Fig. 1 | Mapping core genes and pathways for cancer-intrinsic CTL evasion. **a**, Mouse cell lines screened in this study. Renca, renal carcinoma; B16, melanoma; 4T1 and EMT6, breast carcinoma; CT26 and MC38, colorectal carcinoma. HA and Ova refer to haemagglutinin and ovalbumin antigens, respectively. Cell lines with the C57BL/6 genotype are in grey, and those with the BALB/c genotype are in black. **b**, Workflow for mTKO genome-scale pooled CRISPR screens to identify fitness and CTL-evasion genes. E:T, effector-to-target cell ratio; KO, knockout. The essential gene and non-essential gene distributions are based on gene-level fold-change values, where fold change = $\log_2$(normalized read counts at early or late time points) − $\log_2$(normalized T0 read counts). **c**, Rank-ordered normalized *z*-score (NormZ score) at the mid time point for all six CTL killing screens. Hits at FDR < 5% are highlighted in yellow (resistor genes) and blue (sensitizer genes). The top ten resistor and sensitizer genes are indicated. Dot size is inversely scaled by FDR. **d**, Genetic co-similarity map for cancer-intrinsic CTL evasion. Representative pathways enriched in a cluster are shown on the diagonal axis (FDR < 1%). ETC, electron transport chain; PCC, Pearson correlation coefficient. **e**, Daisy model of gene essentiality, adapted for core cancer-intrinsic CTL-evasion genes. Each cancer cell line is represented as a petal on the flower. **f**, Distribution of cancer-intrinsic CTL-evasion genes at FDR < 5% across the six cell lines. **g**, Pathway themes enriched in core cancer-intrinsic CTL-evasion genes (FDR < 5%). $-\log_{10}(P)$ represents the $-\log_{10}$ of the adjusted *P* value (FDR). Mean percentage overlap refers to the mean of the percentage of overlapping core cancer-intrinsic CTL-evasion and pathway-definition genes across all pathways in a theme. For each theme, the mean number of query genes contained in the pathway/mean pathway term size is displayed to the right of each bar.

perturbation of these genes sensitizes cancer cells to CTL killing across a range of different genetic backgrounds (Extended Data Fig. 4a). One notable exception was the loss of *Adar* in renal carcinoma (Renca) cells, in which *Adar* scored as a fitness gene (Bayes Factor (BF) score = 173; Extended Data Fig. 4b). Consistent with these observations, short hairpin RNA (shRNA) knockdown of *Adar* resulted in the regression of B16 melanomas engrafted on immunocompetent mice (Extended Data Fig. 4c, d).

The observation that regulators of IFNγ signalling can broadly influence cancer-intrinsic CTL evasion motivated us to further examine the genetic determinants that dictate the sensitivity of cancer cells to this cytokine. To this end, we performed a genome-wide CRISPR screen in Renca cells propagated in the presence or absence of recombinant IFNγ, recovering both established suppressors (for example, *Ifngr1* and *Ifngr2*, *Stat1*, *Jak1* and *Jak2*) and sensitizers (for example, *Socs1*, *Ptpn2*) (Fig. 2a). Many of our core cancer-intrinsic CTL-evasion genes were prominent hits in the screen (Extended Data Fig. 5a), confirming the importance of the IFNγ response to the intrinsic CTL-evasion phenotype. These included genes annotated to the autophagy pathway (for example, *Atg3*, *Atg5*, *Atg7*, *Atg10*, *Atg12* and *Atg14*), as well as the poorly characterized lipid-droplet-related gene *Fitm2*, which scored as the top hit (Fig. 2a, Supplementary Table 15).

Fitm2 is required for normal fat storage in adipose tissue in mice[27], but has not been previously associated with IFNγ signalling. We first confirmed the enhanced sensitivity of *Fitm2*-knockout (*Fitm2*Δ) cells to CTL killing with mouse Renca, mouse CT26, and human A375 cells, as well as to IFNγ sensitivity with mouse Renca and mouse B16 cells (Extended Data Fig. 5b, c). After treatment with IFNγ, Renca *Fitm2*Δ cells showed increased visual evidence of cell death relative to control cells (Extended Data Fig. 5d). Notably, B16-Ova cells *Fitm2*Δ

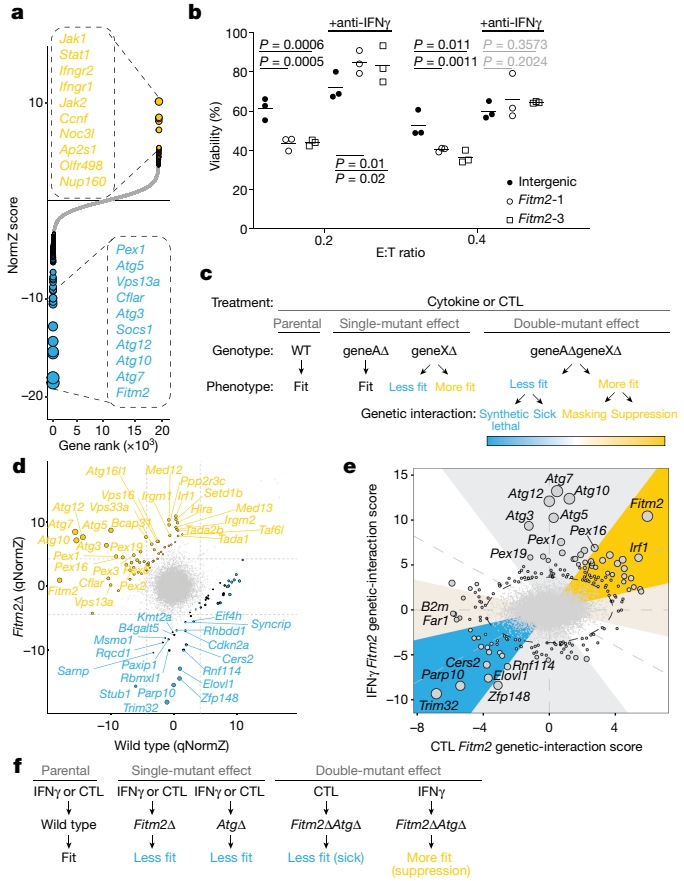

Fig. 2 | IFNγ resistance is a conserved cancer-intrinsic mechanism of CTL evasion. a, Gene-level NormZ scores for genome-wide CRISPR screen in wild-type Renca cells propagated in the presence or absence of IFNγ (10 ng ml^{-1}). Hits at FDR < 5% are highlighted in yellow (resistor genes) and blue (sensitizer genes), and the top ten genes are indicated for each category. Dot size is inversely scaled by FDR. **b**, Viability of B16–Ova cells transduced with gRNAs that target *Fitm2* or intergenic control sites and treated with preactivated OT-1 T cells (CTLs) with or without anti-IFNγ blocking antibodies. Results shown are from a single experiment with three technical replicates. Data are representative of three independent biological replicates. Horizontal lines indicate the mean. *P* values were determined by two-way analysis of variance (ANOVA) with Fisher's least significant difference (LSD) comparison. *P* values indicated in black are significant, in contrast to those in grey, which are not significant. **c**, Schematic outlining genotype-to-phenotype relationship. Positive genetic interactions occur when fitness is better than expected, and are shown in yellow (masking or suppression). Negative genetic interactions occur when fitness is worse than expected, and are shown in blue (sick or synthetic lethal). **d**, Sectored scatter plot of gene-level quantile-normalized *z*-scores (qNormZ) from wild-type and *Fitm2*Δ cells propagated under IFNγ selection pressure. Significant negative and positive genetic interactions (FDR < 5%) are coloured blue and yellow, respectively. Dashed lines indicate median NormZ scores of genetic interactions. **e**, Sunbeam plot of differential gene-level *Fitm2* genetic-interaction scores under IFNγ versus CTL selection pressure. Ellipse (black dashed line), 5% FDR threshold delineated by normal ellipse fit to differential scores. Principal axes (grey dashed lines), lines projecting in direction of each sector (0°, 45°, 90°, 135°, 180°, 225°, 270°, 315°). Sector, area spanning ±22.5° of each sector principal axis: blue and yellow sectors represent consistent hits across both conditions; grey sector represents cytokine-specific effects; tan sector represents CTL-specific effects. Data point sizes are scaled by Euclidean distance from origin. **f**, Schematic outlining select genetic interactions with *Fitm2*. *Atg*Δ, autophagy mutants.

cells displayed similar surface levels of MHC class I (MHC-I) and MHC-I-Ova peptide compared with control cells (Extended Data Fig. 5e, f). These *Fitm2*-related observations were specific to IFNγ, with minimal fitness effects observed after treatment of Renca *Fitm2*Δ cells with TNF (Extended Data Fig. 5g). *Fitm2*Δ-mediated sensitization to CTL killing was abrogated when cells were pretreated with anti-IFNγ blocking antibodies (Fig. 2b), which shows that *Fitm2* is critical for maintaining cell survival after exposure to CTL-produced IFNγ.

To better define the genetic determinants of *Fitm2*-mediated CTL evasion, we mapped genetic interactions for *Fitm2* under IFNγ and CTL selection pressures using genome-wide, pooled CRISPR knockout screens in co-isogenic Renca wild-type and *Fitm2*Δ cells in the presence of IFNγ or activated CTLs. This allowed us to systematically identify secondary genetic perturbations that render *Fitm2*Δ cells less sensitive (that is, positive genetic interactions: more fit or classified as masking or suppression) or more sensitive (that is, negative genetic interactions: less fit or classified as sick or synthetic lethal) to IFNγ or CTL treatment compared to parental wild-type Renca cells (that is, double-mutant interactions) (Fig. 2c). Notably, our *Fitm2*Δ cells exhibited a typical build-up of lipid droplet structures along the endoplasmic reticulum (ER), consistent with the known function of *Fitm2* in the budding of lipid droplets (Extended Data Fig. 6a).

Genetic interactions were calculated by deriving quantile-normalized differential drugZ scores (wild type versus *Fitm2*Δ) for each gene (Fig. 2d, Extended Data Fig. 6b). For both CTL and IFNγ screens, and as expected for this analysis, *Fitm2* itself appeared as a top positive genetic interaction. Of note, strong negative genetic interactions were identified in the IFNγ screen for genes that are involved in regulation of K63-linked protein ubiquitination, including *Trim32*, *Stub1* and *Parp10*, as well as the fatty acid elongation enzyme *Elovl1* (Fig. 2d). Several of these genetic interactions were also identified in the CTL screen at either the gene level (for example, *Trim32*, *Parp10*) or the pathway level (*Far1*) (Extended Data Fig. 6b), suggesting that *Fitm2*Δ cells are susceptible to oxidative proteotoxic and lipotoxic stress, which may occur during exposure to IFNγ. Consistently, whole-transcriptome analysis of *Fitm2*Δ cells treated with IFNγ revealed an upregulation of genes related to ER stress relative to wild-type cells, increased *Xbp1* splicing and increased levels of the ER-stress-related protein BiP (Extended Data Fig. 6c–e, Supplementary Tables 16, 17, Supplementary Information). These results are consistent with a previous report in which *Fitm2* was shown to be a regulator of ER membrane homeostasis that is conserved from yeast to human cells[28].

The analysis of positive genetic interactions also provided insight into the genetic determinants of *Fitm2*-mediated sensitivity to IFNγ, with mutations in autophagy and peroxisomal genes suppressing this phenotype (Fig. 2d, Supplementary Table 18). Indeed, comparison of the rank-ordered IFNγ hits in wild-type and *Fitm2*Δ Renca cells revealed genetic suppression when perturbation of *Fitm2* was combined with perturbation of autophagy genes. For example, *Fitm2*Δ*Atg7*Δ (FDR of around 1.36×10^{-35}), *Fitm2*Δ*Atg10*Δ (FDR ≈ 3.28×10^{-31}), *Fitm2*Δ*Atg12*Δ (FDR ≈ 7.28×10^{-30}), *Fitm2*Δ*Atg5*Δ (FDR ≈ 4.69×10^{-21}), *Fitm2*Δ*Atg3*Δ (FDR ≈ 2.68×10^{-17}) and *Fitm2*Δ*Atg16l1*Δ (FDR ≈ 7.81×10^{-5}) double mutants were particularly resistant to IFNγ-mediated cytotoxicity. This was unexpected, as perturbations in the autophagy and peroxisome pathways were among the strongest sensitizing mutations to IFNγ alone (that is, similar to *Fitm2*) in wild-type Renca cells. These results highlight the profound effects that genetic interactions have in the mediation of cancer-intrinsic CTL evasion, with the mutation of a single gene (*Fitm2*) leading to an autophagy-dependent inverse phenotype.

Autophagy–NF-κβ axis regulates CTL evasion

Notably, perturbations to autophagy only suppressed *Fitm2* sensitization in the presence of IFNγ, and not in the presence of activated CTLs (Fig. 2e, f). This suggests that autophagy perturbation must have other effects that are not mediated by IFNγ—for example, effects mediated by other cytokines released by CTLs. Given the strong enrichment for TNF and NF-κβ signalling pathway genes in our overall core CTL dataset

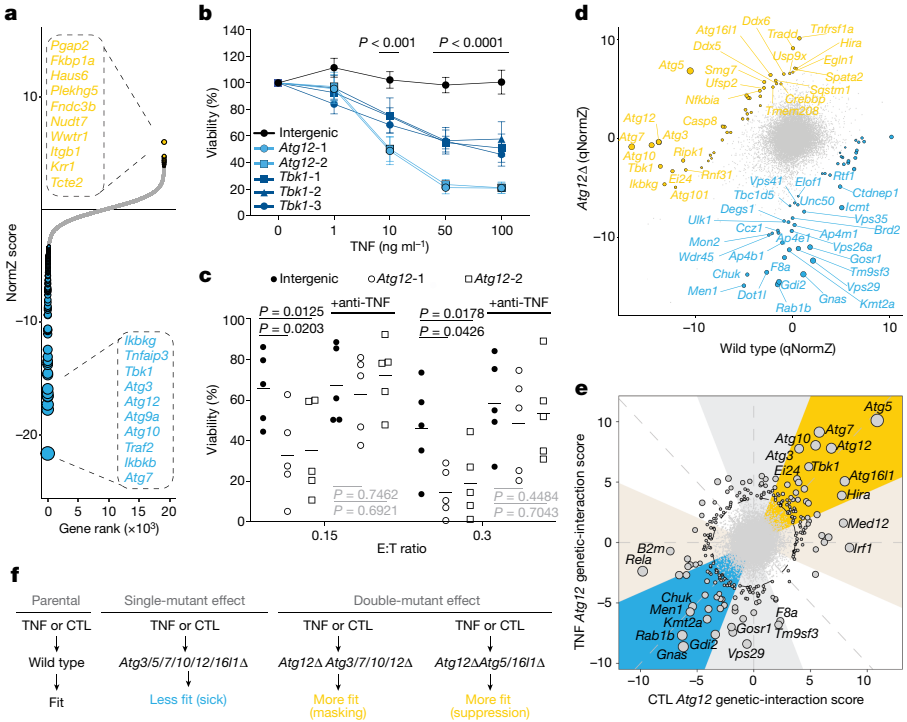

Fig. 3 | A hub of autophagy and NF-κβ signalling mediates cancer-intrinsic CTL evasion. a, Gene-level NormZ scores for genome-wide CRISPR screen in wild-type Renca cells propagated in the presence or absence of TNF (10 ng ml^{-1}). Hits at FDR < 5% are highlighted in yellow (resistor genes) and blue (sensitizer genes), and the top ten genes are indicated for each category. Dot size is inversely scaled by FDR. **b**, Viability of Renca–HA cells transduced with gRNAs that target *Atg12*, *Tbk1* or intergenic control sites after treatment with increasing doses of TNF. Data are mean ±s.e.m. of four (*Tbk1*) or 5 (intergenic, *Atg12*) independent experiments. *P* values were determined by two-way ANOVA with Fisher's LSD comparison. **c**, Viability of Renca–HA cells transduced with gRNAs that target *Atg12* or intergenic control sites and treated with CTLs with or without anti-TNF blocking antibodies. Data are representative of five independent experiments. Horizontal lines indicate the mean. *P* values were determined by two-way ANOVA with Fisher's LSD comparison. *P* values indicated in black are significant, in contrast to those in grey, which are not significant. **d**, Sectored scatter plot of gene-level qNormZ scores between wild-type and *Atg12*Δ cells propagated under TNF selection pressure. Significant negative and positive genetic interactions (FDR < 5%) are coloured blue and yellow, respectively. Dashed lines indicate median NormZ scores of genetic interactions. **e**, Sunbeam plot of differential gene-level *Atg12* genetic-interaction scores under TNF versus CTL selection pressure. Plot features (that is, ellipse, principal axes and sectors) are as described in Fig. 2e. Data point sizes are scaled by Euclidean distance from origin. **f**, Schematic outlining select genetic interactions with *Atg12*.

(Extended Data Fig. 7a)—as well as a significant association between these genes and autophagy in our co-similarity network (Extended Data Fig. 7b, Supplementary Table 19)—we hypothesized that autophagy has a role in mediating resistance to TNF. To test this hypothesis, we performed a genome-wide CRISPR screen in wild-type Renca cells treated with recombinant TNF. This unbiased approach supported our hypothesis, with autophagy and NF-κβ pathway genes scoring as the top sensitizing perturbations (Fig. 3a, Supplementary Table 20). It is noteworthy that neither *Tnfrsf1a* nor *Tnfrsf1b* emerged as resistance genes (that is, alleviating or ameliorating hits), indicating that wild-type Renca cells are not normally wired for TNF-mediated cell death, but can be sensitized through the loss of autophagy or NF-κβ signalling pathways (Supplementary Table 20). We validated these findings in independent experiments, which confirmed that *Atg12*Δ and *Tbk1*Δ cells were highly sensitized to TNF-induced cell death (Fig. 3b). *Atg12*Δ cells were also more sensitive to CTL killing across multiple genetic backgrounds including Renca, EMT6, MC38 (all mouse cell lines) as well as human A375 melanoma cells (Extended Data Fig. 7c–e). Pretreatment of cells with anti-TNF blocking antibodies abrogated *Atg12*-dependent sensitization to CTL killing, verifying the contribution of TNF-mediated death to this phenotype (Fig. 3c, Extended Data Fig. 7f).

We next attempted to pharmacologically replicate our genetic results that demonstrated a role for autophagy genes in sensitivity to TNF-mediated cytotoxicity by using the VPS34 inhibitor autophinib to block autophagy[29], and observed dose-dependent sensitization to CTL killing in our genetically validated mouse MC38 and human A375 cell lines (Extended Data Fig. 8a, b). To determine the generality of these findings, we conducted a drug–cytokine screen across 91 human cell lines. Forty-one cell lines showed synergistic effects (FDR < 0.05) after combinatorial treatment with autophinib and TNF (Extended Data Fig. 8c). Collectively, these results demonstrate the relevance of our findings in human cells.

To further characterize the genetic determinants of autophagy-mediated immune evasion, we mapped *Atg12* genetic interactions under TNF or CTL selection pressure by performing CRISPR screens in Renca co-isogenic wild-type and *Atg12*Δ cells (Extended Data Fig. 9a). As expected, *Atg12* itself appeared as a strong positive genetic interaction (Fig. 3d, Extended Data Fig. 9b, Supplementary Table 21). For both the TNF and the CTL screens, certain NF-κβ-associated genes emerged as either negative or positive genetic interactions. For example, downstream components of the NF-κβ pathway scored as top negative genetic interactions (*Rela*, *Chuk*), whereas upstream regulators of the pathway were more commonly positive genetic interactions (*Tbk1*, *Ikbkg* (also known as *NEMO*), *Ei24*, *Rbck1*, *Ripk1*, *Sharpin*) (Fig. 3d, Extended Data Fig. 9b). This demonstrates the complex relationship between the NF-κβ and autophagy pathways in orchestrating cancer-intrinsic CTL evasion, with our data suggesting that these pathways act in parallel and share upstream regulatory genes. In keeping with this, NF-κβ phosphorylation, nuclear translocation and transcriptional response remained intact when *Atg12*Δ cells were

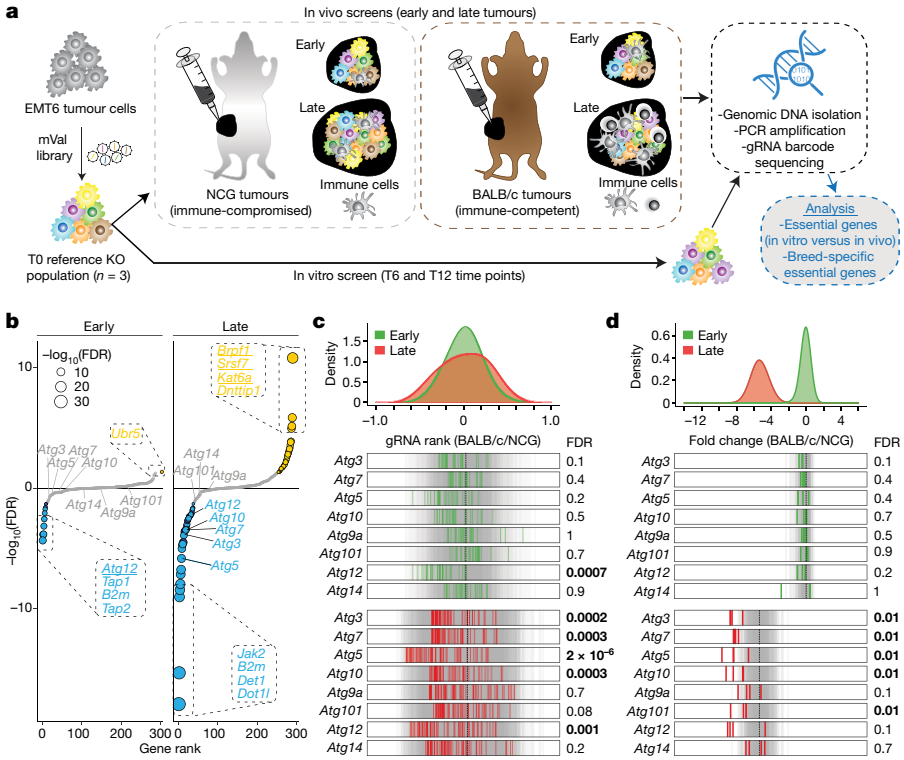

Fig. 4 | In vivo screen validates the role of autophagy as a cancer-intrinsic CTL-evasion pathway. a, Experimental set-up for in vivo CRISPR screen. T refers to time point measured in days after the establishment of the mixed population of EMT6 knockout cells. **b**, Gene-level differential rank between tumours engrafted in BALB/c mice and those engrafted in NCG mice, at early and late time points. Hits at FDR < 5% are highlighted in yellow (resistor genes) and blue (sensitizer genes), markers are scaled by $-\log_{10}$(FDR) and genes validated from the in vitro screen are underlined. **c**, Tumour-level analysis showing distributions and rug plots of differential gRNA ranks for all BALB/c compared to all NCG tumours, targeting autophagy and control genes at early and late time points. The top green and red distributions represent tumour-level data at early and late time points, respectively. In the rug plots (bottom), grey lines indicate targeting control gRNAs and green and red lines represent the average gRNA rank for the indicated gene, for each tumour. Vertical dotted black lines represent the median of control gRNAs. Statistical significance between the autophagy and control genes was determined by two-sided Wilcoxon rank sum test with Benjamini–Hochberg correction (FDR). **d**, gRNA-level analysis showing distributions and rug plots. Top graphs show differential fold change (FC) distributions for early and late tumour time points in different mouse genetic backgrounds (mean($FC_{BALB/c}$) − mean(FC_{NCG})), where $FC_{BALB/c}$ = $\log_2$(BALB/c read counts at early or late time points) − $\log_2$(BALB/c T6-normalized T0 read counts) and FC_{NCG} = $\log_2$(NCG read counts at early or late time points) − $\log_2$(NCG T6-normalized T0 read counts). The rug plots show differential fold change for individual gRNAs that target autophagy and control genes between tumours engrafted in BALB/c mice and those engrafted in NCG mice, at early and late time points. The grey lines indicate targeting control gRNAs. Vertical dotted black lines represent the mean of control gRNAs. Statistical significance between the autophagy and control genes was determined by one-sided Wilcoxon rank-sum test with Holm's multiple testing correction (FDR). FDR values equal to or below 0.01 are indicated in bold.

treated with TNF (Extended Data Fig. 9c, d, Supplementary Table 22, Supplementary Information).

Surprisingly, analysis of *Atg12* genetic interactions revealed a strong inverse phenotype for several members of the autophagy family, most prominently *Atg5* and *Atg16l1* (Fig. 3d, e, Extended Data Fig. 9b); that is, *Atg12*Δ*Atg5*Δ and *Atg12*Δ*Atg16l1*Δ double-mutant cells were strongly resistant to the cytotoxic effects of TNF or CTLs relative to single-mutant cells (Fig. 3f). Both *Atg5* and *Atg16l1* have been reported to function outside of canonical macroautophagy[30], and our results highlight a potential role for these non-canonical functions in immune evasion.

To investigate the role of cancer-intrinsic autophagy within the tumour microenvironment, we next performed an in vivo pooled CRISPR screen in the EMT6 cell model. EMT6 was chosen owing to the strong dependence of this line on autophagy in our in vitro CTL-killing screens, as well as our ability to generate Cas9-expressing tumours in immunocompetent mice. By using our mVal gRNA library targeting the 182 core cancer-intrinsic CTL-evasion genes described above, we propagated EMT6 mutagenized cells in the subcutaneous flanks of immunocompetent BALB/c or immunocompromised NCG mice, sampling tumours at early and late time points to assess the distribution of gRNA barcodes (Fig. 4a). Genes that were previously found to be essential for in vitro EMT6 proliferation were strongly depleted across all samples (Extended Data Fig. 10a–e, Supplementary Table 20), with our screen validating several core cancer-intrinsic CTL-evasion genes, including both sensitizers (*Ago2*, *Med16*, *Tmem127*) and suppressors (*Srsf7*, *Brpf1*, *Kat6a*) (Fig. 4b, Supplementary Table 23). We also observed a strong depletion of gRNAs that target autophagy genes, particularly in the late-stage tumours (Fig. 4c, d, Supplementary Table 23). Overall, these findings show that autophagy has a conserved role in mediating cancer-intrinsic immune evasion within the tumour microenvironment.

Discussion

To explore the functional genomic landscape of cancer-intrinsic CTL evasion, we developed and applied optimized loss-of-function CRISPR–Cas9 genetic screening methods on a genome scale to identify regulators of the response of cancer cells to CTL-mediated killing. By performing screens across our panel of functionally and genetically diverse cell lines, we identified a core conserved set of genes and pathways that broadly mediate cancer-intrinsic CTL evasion. Our study provides a reference set of core CTL-evasion genes and pathways that may inform efforts to develop cancer immunotherapy strategies.

Similar to ongoing large-scale functional genomic efforts to map the dependencies of cancer cell lines, our data reveal the utility of systematically dissecting the complex genetic landscape of cancer-intrinsic immune evasion using a combination of in vitro and in vivo approaches. In particular, we highlight the critical importance of understanding how genetic interactions combine to alter the CTL-evasion phenotype, with pathways such as autophagy exemplifying how strong pleiotropic effects may complicate the application of approaches that target a single gene to cancer immunotherapy.

Online content

Any methods, additional references, Nature Research reporting summaries, source data, extended data, supplementary information, acknowledgements, peer review information; details of author contributions and competing interests; and statements of data and code availability are available at https://doi.org/10.1038/s41586-020-2746-2.

1. Chen, D. S. & Mellman, I. Elements of cancer immunity and the cancer-immune set point. *Nature* **541**, 321–330 (2017).
2. Hegde, P. S. & Chen, D. S. Top 10 challenges in cancer immunotherapy. *Immunity* **52**, 17–35 (2020).
3. Binnewies, M. et al. Understanding the tumor immune environment (TIME) for effective therapy. *Nat. Med.* **24**, 541–550 (2018).
4. Hugo, W. et al. Genomic and transcriptomic features of response to anti-pd-1 therapy in metastatic melanoma. *Cell* **165**, 35–44 (2016).
5. Rooney, M. S., Shukla, S. A., Wu, C. J., Getz, G. & Hacohen, N. Molecular and genetic properties of tumors associated with local immune cytolytic activity. *Cell* **160**, 48–61 (2015).
6. Zaretsky, J. M. et al. Mutations associated with acquired resistance to PD-1 blockade in melanoma. *N. Engl. J. Med.* **375**, 819–829 (2016).
7. Kearney, C. J. et al. Tumor immune evasion arises through loss of TNF sensitivity. *Sci. Immunol.* **3**, eaar3451 (2018).
8. Manguso, R. T. et al. In vivo CRISPR screening identifies Ptpn2 as a cancer immunotherapy target. *Nature* **547**, 413–418 (2017).
9. Pan, D. et al. A major chromatin regulator determines resistance of tumor cells to T cell-mediated killing. *Science* **359**, 770–775 (2018).
10. Patel, S. J. et al. Identification of essential genes for cancer immunotherapy. *Nature* **548**, 537–542 (2017).
11. Vredevoogd, D. W. et al. Augmenting immunotherapy impact by lowering tumor TNF cytotoxicity threshold. *Cell* **178**, 585–599 (2019).
12. Hart, T. et al. Evaluation and design of genome-wide CRISPR/SpCas9 knockout screens. *G3* **7**, 2719–2727 (2017).
13. Hart, T., Brown, K. R., Sircoulomb, F., Rottapel, R. & Moffat, J. Measuring error rates in genomic perturbation screens: gold standards for human functional genomics. *Mol. Syst. Biol.* **10**, 733 (2014).
14. Hart, T. et al. High-resolution CRISPR screens reveal fitness genes and genotype-specific cancer liabilities. *Cell* **163**, 1515–1526 (2015).
15. Hart, T. & Moffat, J. BAGEL: a computational framework for identifying essential genes from pooled library screens. *BMC Bioinformatics* **17**, 164 (2016).
16. Li, B. et al. A comprehensive mouse transcriptomic BodyMap across 17 tissues by RNA-seq. *Sci. Rep.* **7**, 4200 (2017).
17. Söllner, J. F. et al. An RNA-seq atlas of gene expression in mouse and rat normal tissues. *Sci. Data* **4**, 170185 (2017).
18. Zimmermann, M. et al. CRISPR screens identify genomic ribonucleotides as a source of PARP-trapping lesions. *Nature* **559**, 285–289 (2018).
19. Costanzo, M. et al. A global genetic interaction network maps a wiring diagram of cellular function. *Science* **353**, aaf1420 (2016).
20. Weichhart, T. & Säemann, M. D. The multiple facets of mTOR in immunity. *Trends Immunol.* **30**, 218–226 (2009).
21. Gerlinger, M. et al. Intratumor heterogeneity and branched evolution revealed by multiregion sequencing. *N. Engl. J. Med.* **366**, 883–892 (2012).
22. Thorsson, V. et al. The immune landscape of cancer. *Immunity* **48**, 812–830.e14 (2018).
23. Smith, C. C. et al. Endogenous retroviral signatures predict immunotherapy response in clear cell renal cell carcinoma. *J. Clin. Invest.* **128**, 4804–4820 (2018).
24. Liddicoat, B. J. et al. RNA editing by ADAR1 prevents MDA5 sensing of endogenous dsRNA as nonself. *Science* **349**, 1115–1120 (2015).
25. Starr, R. et al. A family of cytokine-inducible inhibitors of signalling. *Nature* **387**, 917–921 (1997).
26. Ishizuka, J. J. et al. Loss of ADAR1 in tumours overcomes resistance to immune checkpoint blockade. *Nature* **565**, 43–48 (2019).
27. Miranda, D. A. et al. Fat storage-inducing transmembrane protein 2 is required for normal fat storage in adipose tissue. *J. Biol. Chem.* **289**, 9560–9572 (2014).
28. Becuwe, M. et al. FIT2 is a lipid phosphate phosphatase crucial for endoplasmic reticulum homeostasis. Preprint at *bioRxiv* https://doi.org/10.1101/291765 (2018).
29. Robke, L. et al. Phenotypic identification of a novel autophagy inhibitor chemotype targeting lipid kinase VPS34. *Angew. Chem. Int. Edn Engl.* **56**, 8153–8157 (2017).
30. Tan, J. M. J., Mellouk, N. & Brumell, J. H. An autophagy-independent role for ATG16L1: promoting lysosome-mediated plasma membrane repair. *Autophagy* **15**, 932–933 (2019).

Publisher's note Springer Nature remains neutral with regard to jurisdictional claims in published maps and institutional affiliations.

© The Author(s), under exclusive licence to Springer Nature Limited 2020

Methods

Plasmids

Lenti-HA-RFP was generated by PCR amplification of the Puerto Rico influenza A strain 8 haemagglutinin sequence (a gift from T. Griffith) followed by ligation into the lentiCas9-EGFP (Addgene 63592) backbone by restriction enzyme digestion to remove the Cas9 open reading frame and Gibson assembly. Monomeric RFP (mRFP) was subsequently inserted and replaced EGFP by restriction enzyme digestion and Gibson assembly. Lenti-OVA was generated internally, with the OVA sequence[31] cloned into a pLVX-EF1a-IRES-neo backbone and Flag-tagged in the N terminus (pLVX-EF1a-IRES-neo: OVA, Flag N-term). Lenti-Cas9-2A-Blast plasmid (Addgene 73310) was used to make Cas9 stably expressing cell lines. The lentiviral firefly luciferase construct (PGK-GFP-IRES-LUCIFERASE) was used to make cell lines that stably express luciferase. The modified lentiCRISPRv2 (ref. [12]) and pLCKO2 plasmids[32] (Addgene 125518) were used for expression of individual gRNAs in native or Cas9-expressing cell lines, respectively.

Cell lines

A complete list of cell lines, including the 91 used in the autophinib screen, can be found in the Supplementary Information. Commonly used lines include Renca, CT26, B16, MC38, HEK293T, 4T1 and EMT6, and were originally purchased from American Type Culture Collection (ATCC). The 4T1 and EMT6 cell lines were gifts from W. Chan and D. Morris, respectively. These lines were maintained in RPMI 1640 supplemented with 10% FBS and 1% penicillin–streptomycin (Life Science Technologies). Cells were cultured at 37 °C, 5% CO_2. Cell lines were authenticated using whole-transcriptomic analysis. No short tandem repeat (STR) analyses were performed on the above cell lines. Mycoplasma testing was routinely performed. U-118 MG (contained in the 91-cell-line panel for the autophinib screen) is the only cell line used in this study that appears on the commonly misidentified list. This line was purchased from ATCC and verified by STR analysis.

HA-expressing cell lines were generated in the Renca, CT26, 4T1 and EMT6 backgrounds via transduction with lenti-HA-RFP. Successfully transduced cells were selected via flow cytometry and subjected to limiting dilution and single-cell clonal expansion. Ova-expressing cell lines were generated in the B16 and MC38 backgrounds via transduction with lenti-Ova followed by flow cytometry to obtain an Ova^{hi} polyclonal population. HA- and Ova-expressing cell lines were periodically re-sorted by flow cytometry to maintain cells with high expression levels. In addition, for validation experiments, B16F10–Ova and MC38–Ova cell lines were engineered to stably express TdTomato (pLVX-EF1a-IRES-hyg-tdTomato), whereas Renca–HA, CT26–HA, 4T1–HA and EMT6–HA were engineered to stably express firefly luciferase (PGK-GFP-IRES-LUCIFERASE). All lines were sorted for high expression.

Knockout cell lines were generated by electroporation using the Neon Transfection System (Invitrogen) following the manufacturer's instructions. In brief, high-quality modified LCV2 or pLCKO plasmids targeting a gene of interest were prepared using the PureLink Plasmid Midiprep/Maxiprep Kit (Invitrogen), and electroporated into Renca or Renca-HA^{Cas9+}, respectively. Twenty-four hours after electroporation cells were puromycin-selected for 72 h. Selected cells were then subjected to limiting dilution and single-cell clonal expansion. Genomic DNA from selected clones was extracted using the QIAamp DNA Blood Mini kit (Qiagen) and gRNA target regions were PCR-amplified and analysed by Sanger sequencing. Confirmation of gene knockout was performed using TIDE (https://tide.nki.nl/) to identify out-of-frame insertion-and-deletion mutations. CRISPR-mediated gene knockouts were also verified by manual inspection of the aligned RNA sequencing (RNA-seq) reads at the gRNA target sites in the Integrative Genomics Viewer (IGV), when RNA-seq data were available (for example, Renca *Fitm2*Δ and *Atg12*Δ knockout cells).

Animals

The use of animals in this study followed the guidelines of the Canadian Council on Animal Care, Ontario's Animals for Research Act, The Guide for the Care and Use of Laboratory Animals, Cambridge Public Health Laboratory Animal Ordinances and the USDA's Animal Welfare Act. The study was approved by the University Animal Care Committee at the University of Toronto and the Institutional Animal Care and Use Committee at Agios Pharmaceuticals. At the University of Toronto, mice were housed at approximately 22 ± 2 °C, humidity 45% on a 14-h light, 10-h dark cycle. At Agios, mice were housed at approximately 21 ± 3 °C, 30–70% humidity on a 12-h light/dark cycle. Two- to-twelve-month-old female or male Clone 4 (CL4) (CBy.Cg-Thy1aTg(TcraCl4,TcrbCl4)1Shrm/ShrmJ, stock no. 005307) and 3–6-month-old female OT-1 (C57BL/6-Tg(TcraTcrb)1100Mjb/J, stock no. 003831) T cell receptor transgenic mice were used, being purchased from The Jackson Laboratory (www.jax.org) with a breeding colony maintained. CL4 genotyping was performed according to The Jackson Laboratory protocols. Eight-to-twelve-week-old female C57BL/6j and NSG mice were purchased and used from The Jackson Laboratory and housed under specific pathogen-free conditions in the Agios animal care facility. Eight-to-sixteen-week-old female NCG (NOD-*Prkdc*^{em26Cd52}*Il2rg*^{em26Cd22}/NjuCrl, strain no. 572) and BALB-c mice were used and purchased from Charles River Laboratory.

Quantitative PCR analyses

RNA was extracted using the Qiagen RNeasy Plus Mini Kit according to the manufacturer's protocol (74136, Qiagen). cDNA was synthesized by converting extracted RNA using the RNA to cDNA EcoDry Premix (Oligo dT) according to the manufacturer's protocol (629543, Takara). Relative gene expression levels were monitored using the following Taqman assays from Applied Biosystems: ADAR1 (Mm00508001_m1) and PPIA (Mm02342430_g1) using Advanced Fast Master Mix (4444557, Applied Biosystems). CT values were normalized to PPIA as the endogenous control.

mTKO and validation library construction

All 94,528 gRNA sequences for the mTKO library were designed in an analogous manner to the human TKOv3 library and cloned into the pLCKO2 vector as previously described[12]. The cloned plasmid pool yielded a 2,300-fold representation of the library.

For the validation library (also referred to as mVal), gRNAs targeting the 182 core cancer-intrinsic CTL-evasion genes were selected from the mTKO library. The top four best-performing gRNAs displaying the most significant depletion (sensitizers) or enrichment (suppressors) in fold change between CTL-treated versus untreated populations across the genome-wide screens were selected for each gene. An additional 728 control gRNAs were included in the library targeting 182 genes (4 gRNAs per gene) that displayed no significant proliferation (Bayes Factor (BF) score, see 'Data processing for pooled CRISPR screens') or immune-evasion (NormZ, see 'Analysis of cancer-intrinsic CTL-evasion genes') fitness profile and were expressed across all cell lines. Cloning of the mVal library was performed in an analogous manner to the mTKO library, as described above. Oligos were obtained from Agilent and the library was cloned at 233-fold representation.

In vitro genome-wide and mini-validation CRISPR screens

Cas9-expressing cells were infected with the mTKO lentiviral library at a multiplicity of infection (MOI) of around 0.5. Twenty-four hours after infection, cells were selected with puromycin for 48–96 h. Selected cells were divided into a control and an experimental group with three replicates each and maintained at around a 200-fold library coverage throughout the screens. For T cell killing screens, the experimental groups were treated with preactivated CL4 or OT-1 $CD8^+$ T cells to achieve approximately 50% or higher cytotoxicity (determined by

microscopic evaluation), with control groups being treated with wild-type $CD8^+$ T cells (B16–Ova, MC38–Ova) or left untreated (Renca–HA, EMT6–HA, 4T1–HA, CT26–HA). For cytokine screens, the experimental groups were treated with recombinant TNF (10 ng/ml) or IFNγ (10 ng ml) to achieve approximately 50% or higher cytotoxicity (determined by microscopic evaluation). Treatments were repeated 2–3 times throughout the course of each screen. Screens in isogenic mutant lines were performed in an analogous fashion, as above. At each passage, cell pellets were collected at around a 200-fold library coverage for genomic DNA extraction, starting at day 0 after selection. Genomic DNA was extracted using the Wizard Genomic DNA Purification kit (Promega) according to the manufacturer's instructions. gRNAs were amplified as described previously[32]. The resulting libraries were sequenced on an Illumina HiSeq2500. For each screen, we sequenced a mid and end time point (except *Fitm2* CTL-treated screen), defined as the population of cells following 1–2 and 2–3 treatment rounds, respectively.

CTL killing validation screens were performed across our cell line panel using the mVal library in an analogous fashion to that described above but at more than 500× representation.

Data processing for pooled CRISPR screens

For each sample, reads were preprocessed by locating the first 8 bp of one of the three anchors used in the barcoding primers (U6, tracr or pLCKO tracr), and extracting the 20 bp preceding the anchor using a bespoke Perl script. We allowed up to two mismatches during the anchor search. The untrimmed reads were retained for quality control; the median ratio of reads with unmatched anchors was 1.0% for the genome-wide library, and 5.3% for the validation library. After trimming, a quality control alignment was performed using Bowtie v. 0.12.8 (allowing for a maximum of two mismatches, ignoring qualities). On average, 89.7% of the trimmed reads aligned for the mouse TKO screens, and 95.4% of the reads aligned for the validation screens.

For each sample, all available reads were combined from different sequencing runs if applicable and aligned using Bowtie as described above, and gRNAs were tallied. Read counts for all samples in a screen were combined in a matrix and normalized to 10 million reads per sample by dividing each read count by the sum of all read counts in the sample and then multiplying by 10 million. Fold change is calculated against a reference sample (usually T0). Bayes Factor (BF) scores were calculated as previously described[12,14,15].

Analysis of cancer-intrinsic CTL-evasion genes

To measure the effect of gene knockout on cancer cell fitness during treatment with CTLs, we compared paired screens of cell lines cultured with and without CTLs using the drugZ version 1.0 pipeline (Python v.3.7.1) for two different time points (mid, end)[33]. An FDR threshold of 5% for sensitizer and resistor genes was used.

For cancer-intrinsic CTL-evasion genes, we identified and visualized significantly enriched pathways for each screen using GSEA (GSEA v3.0)[34]. GSEA was performed using a preranked gene list sorted on the basis of mid-time point drugZ scores as input. The pathway database was obtained from the laboratory of G.B. (http://download.baderlab.org/EM_Genesets/), and comprised pathways from Reactome, NCI Pathway Interaction Database, Gene Ontology (GO) Biological Processes (BP), HumanCyc, MSigDB, Netpath and Panther[35]. GO terms inferred from electronic annotations were excluded. Only pathways with between 8 and 200 genes were included. Enrichments were visualized using Cytoscape (v.3.7.1) with the Enrichment Map plug-in (v.3.5.1), in which nodes represent pathways and edges connect pathways with overlapping genes. Nodes are connected by an edge if they share gene set similarity ≥ 0.375. Clusters of related nodes were circled using the AutoAnnotate plug-in v.1.3 in Cytoscape and given a general pathway label. Pathways are shown if they were enriched in at least three or more screens at an FDR of <5% (blue, sensitizer; yellow, suppressor).

Core cancer-intrinsic CTL-evasion genes were identified as those that were hits in at least three cell lines (FDR < 5%). Pathway enrichment for these genes was performed using g:Profiler (accessed around 3 October 2018). Reactome and GO:BP pathways with between 3 and 200 genes were included. Enriched pathways were visualized using Cytoscape, and the AutoAnnotate plug-in (v.1.3) was used to find pathway themes. A pathway similarity of 0.3 was used to connect related nodes. For each pathway in each theme, the percentage overlap (that is, percentage of core killing genes found in that pathway) was computed as: overlap size/gene set size. The mean percentage overlap was computed over all pathways in the theme, and the *P* value was set to be the minimum *P* value over all pathways in the theme. The bar plot displays the mean percentage overlap for each theme and is ordered and coloured according to the maximum $-\log_{10}(P \text{ value})$.

Rank order of core cancer-intrinsic CTL-evasion genes

The rank product was calculated by multiplying the rank of a given gene across each of the six screens and raising the product to the power of multiplicative inverse of the number of screens (that is, 1/6):

$$\text{Rank.Product} = (\text{Rank1} \times \text{Rank2} \times \text{Rank3} \times \text{Rank4} \times \text{Rank5} \times \text{Rank6})^{1/6}$$

To calculate *P* values, 1,000 random sets of 182 rows by 6 columns were generated. Each column in each set contained values between 1 and 182. The rank product was calculated for each of the sets and combined into a large matrix of 182 rows by 1,000 columns of random rank products. In parallel, the screen rank products were converted into a large matrix of the same dimensions as the random sets by replicating the rank products for the 182 genes 1,000 times (resulting again in 182 rows by 1,000 columns with the same rank product per column). *P* values were then calculated by subtracting the screen data matrix (182 rows × 1,000 columns) from the random set matrix (182 rows × 1,000 columns) element-wise, then summing the resulting differences across every row and dividing by 1,000.

Co-similarity analysis

NormZ profiles for all six cell lines at mid and end time points were obtained using drugZ as described above, resulting in a total of 12 data points for each gene. We subsequently calculated the Pearson correlation coefficients (PCCs) between all possible gene pair combinations across the 12 data points. To reduce the number of associations between genes lacking phenotypes in our screen, we filtered the resultant matrix of PCCs to include only genes with three or more significant drugZ scores at an FDR of 5%. This threshold was determined using a benchmarking analysis that used a log-likelihood score (LLS) to quantify functional enrichment in the highly correlated gene pairs across various data point thresholds (number of data points required, N_{dp}), as previously described[36].

In brief, the LLS is represented by the following formula:

$$\text{LLS} = \log\left(\frac{P(L|E)/P(\neg L|E)}{P(L)/P(\neg L)}\right),$$

in which *E* represents the top-ranked gene pairs by PCC (for example, top 1,000 gene pairs above threshold N_{dp}), $P(L|E)$ represents the frequency of gene pairs in the filtered matrix belonging to the same functional pathway using the Bader laboratory pathway database ('co-annotated'), and $P(\neg L|E)$ represents gene pairs that are present in the pathway but not co-annotated. Therefore, $P(L|E)/P(\neg L|E)$ represents the odds ratio (OR) for gene pair co-annotation at the given threshold. In the denominator, $P(L)$ represents the frequency of all co-annotated gene pairs in the unfiltered matrix, $P(\neg L)$ represents the frequency of pairs lacking co-annotation, and $P(L)/P(\neg L)$ measures the OR of functional enrichment in the unfiltered matrix, or the background OR.

Taking the log of the two OR values produces a LLS for functional enrichment in the filtered gene pairs at the given threshold, N_{dp}.

To account for extreme filtering effects that may artificially inflate the score, we adjusted the LLS with a filtering parameter and termed this the conditional LLS. To achieve this, we separated the LLS into two components: a conditional LLS that represents functional enrichment (that is, LLS) after controlling for the filtering effect, and a significance-based filtering effect. This is represented by the following formula:

$$\begin{aligned}\mathrm{LLS} &= \log\left(\frac{P(L|E)/P(\neg L|E)}{P(L)/P(\neg L)}\right)\\ &= \log\left(\frac{P(L|E)/P(\neg L|E)}{P(L|F)/P(\neg L|F)}\right) + \log\left(\frac{P(L|F)/P(\neg L|F)}{P(L)/P(\neg L)}\right)\\ &= \mathrm{LLS}_{\mathrm{conditional}} + \text{filtering effect},\end{aligned}$$

Here, we multiplied the previously introduced LLS formula by $P(L|F)/P(\neg L|F)$, which represents the OR of functional enrichment in the gene list filtered by the data point threshold. Consequently, the right term (that is, filtering effect) captures the functional bias of filtering genes using a specific data point threshold, whereas the left term explains the network predictive power (that is, LLS) after removing this filtering bias.

To establish a threshold N_{dp}, we calculated the conditional LLS of the first 1,000 gene pairs, ordered from highest to lowest PCC, for all data point thresholds. We also calculated the percentage genome coverage after filtering, defined as the number of genes in the dataset after filtering over the total number of genes in the mouse genome, to determine the optimal threshold that maintains both high conditional LLS and genome coverage. A threshold of three data points best fulfilled these criteria, resulting in a final matrix of 548 genes. To determine the functional prediction performance of this matrix, we quantified the LLS using independent annotations defined by the KEGG and CORUM protein complex databases for all pairwise gene combinations amongst these 548 genes[37,38].

Next, we plotted a co-similarity matrix, consisting of PCC values between the 548 genes, and arranged by hierarchical clustering using Euclidian distance and average linkage methods. To select the optimal number of clusters, we evaluated the functional enrichment of various numbers of clusters by measuring the enrichment ratio of gene pairs within clusters versus random probability.

The enrichment ratio was defined as: (positive interactions/number of gene pairs within a cluster)/(positive interactions across genome/number of gene pairs across genome).

To define positive interactions, we only considered pathway terms (that is, gene sets) containing fewer than 50 genes to avoid inclusion of overly general pathways. Dividing into 37 clusters provided the strongest functional enrichment. To identify functional terms that best describe each cluster, we calculated Benjamini–Hochberg-corrected *P* values for functional enrichment with GO-BP terms using Fisher's exact test. A representative pathway term enriched at an FDR of < 1% was chosen to label each cluster. For clusters without any significant enrichment, the cluster ID number was displayed. A cluster–cluster interaction diagram was then generated using the mean PCC of pairwise interactions between genes in cluster pairs.

A subnetwork for autophagy genes and their interactors in the co-similarity network was visualized using Cytoscape. Nodes represent genes annotated to the autophagy pathway (GO:0006914) and their interactors. Interactors connected to at least two autophagy genes were shown in the network.

Genetic interaction analysis

Genetic interactions for *Atg12* and *Fitm2* under cytokine or CTL selection pressures were calculated by computing quantile-normalized differential NormZ scores between mutant versus wild-type cells. Quantile normalization was conducted for each treatment set separately by including data from all screens under a given selection pressure; for CTLs (wild type; *Fitm2*; *Atg12*); TNF (wild type; *Atg12*); and IFNγ (wild type; *Fitm2*).

The difference (*D*) between wild-type gene effect (normZ_{WT}) and mutant gene effect (normZ_{KO}) was calculated for all mTKO targeted genes and converted to a *z*-score as shown below:

$$D = \mathrm{normZ}_{KO} - \mathrm{normZ}_{WT}$$

$$\text{Genetic interaction score } (z) = \frac{D - \mathrm{Mean}_D}{\mathrm{STD}_D}$$

A negative score reflects that perturbation of the gene results in a reduced fitness in the context of the mutant background, whereas a positive score reflects improved fitness. Finally, we calculated *P* values corresponding to the *z*-score, and convert to FDR by Benjamini–Hochberg correction.

RNA-seq

To obtain RNA for sequencing, $0.5–1 \times 10^6$ cells transduced with lentivirus bearing gRNAs targeting *Atg12*, *Fitm2* or intergenic control regions were seeded onto 6-well or 10-cm plates and cultured in complete medium until confluent. As indicated, clonal *Atg12*Δ and *Fitm2*Δ cells were also used. For baseline cell line expression analysis, cells were cultured for 48 h in duplicates. For *Atg12*Δ and *Fitm2*Δ studies, experiments were done in triplicate and cells were challenged with TNF (10 ng/ml) for 12 h or IFNγ (10 ng/ml) for 48 h, with cytokine-free medium serving as control. For all experiments, RNA was extracted from cultured cells using the RNeasy Plus Mini Kit (Qiagen) according to the manufacturer's protocol. In brief, cells were lysed on ice in RTL plus buffer (Qiagen) and passed through QIAshredder columns. Supernatant was then transferred to RNeasy spin columns and an on-column DNase treatment was performed using the RNase-free DNase set (Qiagen).

RNA-seq data processing

Libraries were sequenced with single-end 76-bp reads on a NextSeq500 (baseline expression analysis) or paired-end 2 × 100-bp reads on an Illumina NovaSeq6000 (*Atg12*-mutant and *Fitm2*-mutant studies) sequencer using an S2 flowcell. Samples were mixed to obtain an average of 25 million single-end or 35 million paired-end clusters that passed filtering. Reads shorter than 36 bp on either read 1 or read 2 were removed before mapping. Reads were aligned to reference genome mm10 and Gencode vM12 gene models using the STAR short-read aligner (v.2.6.1b)[39]. For samples run on the NextSeq500, an average of 82.5% of filtered reads mapped uniquely (min 81.5%, max 83.8%), and an average of 90.8% of the filtered NovaSeq reads mapped uniquely (min 86.3%, max 93.1%). The gene-level read counts from each sample, computed by STAR, were merged into a single matrix using R. Finally, cufflinks (v.2.2.1) was used to generate a matrix of FPKM values for all samples using default parameters. The raw and processed data have been deposited in the Gene Expression Omnibus (GEO) database.

RNA-seq analysis

For *Atg12* and *Fitm2* knockout experiments, differentially expressed genes were identified using the Bioconductor packages limma (v.3.32.10) and edgeR (v.3.24.3). The read count matrix was filtered using the filterByExpr() function using default parameters. Principal component analysis was performed to examine the main treatment effects, and to exclude the presence of confounding batch effects, using the base R function prcomp(). Samples were normalized using calcNormFactors(method = "TMM") from edgeR and transformed to $\log_2$ using the voom function in limma. Next, a design matrix was specified to fit coefficients for the CRISPR knockouts, presence or

absence of cytokine, and an interaction term to examine differences in the cytokine effect in the mutant backgrounds. Differentially expressed genes were extracted using the topTable function in limma with absolute $\log_2$(fold change) > 0.58 (where fold change = $\log_2$(KO or WT read counts ± cytokine) − $\log_2$(WT read counts)) and adjusted *P* value < 0.05. Volcano plots were generated for visualization, with genes displaying an absolute fold change > 0.4 and a *P* value $<10^{-6}$ being highlighted. Pathway analysis was performed on differentially expressed genes using these thresholds with g:Profiler, as described above.

To quantify the relative expression of the short and long splice forms of *Xbp1*, the base-level depth of sequence reads through exon 4 (chr11:5524239-5524384) of *Xbp1* was extracted from the aligned BAM files using samtools depth. The short splice form is characterized by splicing out 26 base pairs between chr11:5524277-5524304. Thus, the ratio of short to long form is computed as: ratio = 1 − mean.26bp/(mean(upstream, downstream)). Differences in mean ratios between conditions were assessed using a Student's *t*-test.

Isolation and activation of CD8$^+$ T cells

Naive CL4 or OT-1 CD8$^+$ T cells were magnetically separated from freshly extracted CL4 mouse spleens using an antibody magnetic separation kit (130-096-543, Miltenyi or 19853, StemCell). Immediately following isolation, T cells were activated and expanded with CD3/CD28 beads according to the manufacturer's protocol (130-093-627, Miltenyi or 11453D, Gibco). Activated CD8$^+$ T cells were cultured for 4–6 days before use in all experiments.

In vitro T cell cytotoxicity assay

HA- or Ova-expressing Cas9$^+$ cancer cell lines were transduced with lentivirus bearing gRNAs targeting genes of interest or intergenic control regions. Transduced cells were selected with puromycin for around 72 h and seeded into 24- (25,000–50,000 cells per well) or 96- (1,500–5,000 cells per well) well plates in duplicates or triplicates. Following overnight incubation, cells were treated with preactivated CL4 or OT-1 CD8$^+$ T cells at increasing effector-to-target ratios for around 48 h.

At the end point, CD8$^+$ T cells and dead cancer cells were removed by gentle PBS wash, with cancer cell viability assessed by counting the remaining adherent cells in each well on a Coulter counter (24-well plates), via bioluminescence using a microtitre plate reader (96-well plate) or using CellTiter-Glo (CTG) reagent according to the manufacturer's instructions (G7570, Promega). For selected experiments, cancer cell viability was also monitored by live-cell fluorescent microscopy using the IncuCyte. In all cases, cell viability relative to untreated control cells is shown.

For selected experiments, cancer cells were preincubated for 30 min with 100 μg/ml anti-TNF (MP6-XT22, Biolegend 506331) or anti-IFNγ (XMG1.2, Biolegend 505834) antibodies before addition of T cells to neutralize these cytokines during co-culture.

Cytokine dose-response assay

Cancer cells were transduced and seeded in 96-well plates as per the in vitro T cell cytotoxicity assay. Twenty-four hours after seeding, cells were treated with increasing doses of recombinant TNF (1–100 ng/ml) or IFNγ [1–100 ng/ml) for 72 h. Cell viability was measured via bioluminescence using a microtitre plate reader or by live-cell fluorescent microscopy using the IncuCyte for selected experiments. In all cases, cell viability relative to untreated controls cells is shown.

In vitro studies in human cancer cell lines

A375 (ATCC, CRL-1619) knockout cell lines were generated by electroporating Cas9 guide-conjugated RNPs as per a previous study[40] using the 4D-Nucleofector system (Lonza) and Lonza optimized protocol for A375 cells. In brief, RNPs were produced by incubating 2 sgRNAs with Cas9 (Thermo Fisher Scientific, A36499) at a final 3:1 molar ratio, and electroporated into A375 cells using the SF cell line solution (Lonza, VAXC-2032) with the FF-120 program. Each electroporation well contains 2×10^5 cells, 180 pmol Cas9 and 540 pmol sgRNA (2 guides combined per electroporation targeting either intergenic regions or the human gene of interest as follows sgIntergenic-1 and 2: GGGGCC ACTAGGGACAGGAT; GTCACCAATCCTGTCCCTAG, sgAtg12-1 and 2: CTCCCCAGAAACAACCACCC; CCTCCAGCAGCAATTGAAGT, sgFitm2-1 and 2: GAGGTAGCTCTCGGGCAACG; CGGGGTGCACTCACACGTTG). Twenty-four hours after electroporation cells were assessed for knockout by western and/or quantitative (q)PCR and used in the final assays within five passages from electroporation.

Human co-culture was performed by culturing A375 cells with anti-WT1 T cells (Astarte Biologicals, 1089-4040SE18) in the presence of 2 ng/ml of human recombinant IL-2 and increasing concentrations of autophinib (0–1,000 nM) for 60 h at an E:T ratio of 10:1. Similarly to mouse co-culture studies, CD8$^+$ T cells and dead cancer cells were removed by gentle PBS wash and remaining viable cells were assessed using CTG reagent according to the manufacturer's instructions (Promega, G7570).

A panel of 91 human cancer cell lines were seeded in 96-well plates in the recommended medium for each cell line and at densities optimized for each cell line and ranging from 2,000 to 6,000 cells per well. Twenty-four hours after seeding, cells were treated with human recombinant TNF (Invitrogen,10602HNAE50) ranging from 0 to 100 U/ml and/or autophinib (Tocris Bioscience, 63-245-0) ranging from 0–1,000 nM for a total of 72 h. Cell viability was then assessed using CTG reagent according to the manufacturer's instructions (Promega, G7570) at $T = 0$ and at the end of the experiment, $T = 72$ h.

Growth rates (μ) were calculated using the following formula: $\mu = \mathrm{LN}(T_{\text{end-blank}})/(T_{0\text{-blank}})]/\text{time (h)}$. $\mu/\mu_{\max}$ calculations were used to compare growth rates of drug-treated to vehicle-treated cells, where maximum growth is observed in vehicle (DMSO)-treated cells.

Synergy scores between TNF and autophinib were computed using the following model:

$$1-\mu(c_A, c_T)/\mu_{\max} = 1-\mu(0, c_T)/\mu_{\max} + 1-\mu(c_A, 0)/\mu_{\max} + s_{AT}$$

in which $\mu(c_A,c_T)$ is the growth rate of cells treated with concentrations c_A and c_T for autophinib and TNF, respectively. The residual, s_{AT}, captures the effect of both treatments at concentrations c_A and c_T. The average synergy was computed across all concentrations of autophinib and TNF, in which M is the total number of conditions:

$$s = \frac{1}{M}\sum_{A,T} s_{AT}$$

Live-cell imaging

For select cytokine sensitivity assays, TdTomato-expressing cancer cells were plated in clear-bottom 96-well plates (3904, Corning) at optimized densities, treated with increasing concentrations of IFNγ (78021.2, StemCell) or TNF (315-01A, Peprotech) and imaged every 2 h for at least 72 h (IncucyteS3 or Zoom, Essen Bioscience). The images were analysed using IncuCyte software (IncuCyte S3 v.2018A or Zoom v.2016A, Essen Biosciences) and the confluency of the red fluorescent cells was calculated.

Western blot analyses

For experiments assessing protein levels of NF-κβ, NRF2 and autophagy proteins, wild-type versus clonal *Atg12*Δ or *Atg7*Δ isogeneic Renca–HA cells were used. As indicated, polyclonal knockout populations were also used by transducing Renca cells with intergenic versus *Atg12* gRNAs. A total of 1.5×10^6 cells were seeded into 10-cm plates and cultured for 48 h, followed by treatment with TNF (100 ng/ml) for 30 min. Nuclear and cytoplasmic protein fractions were generated using the NE-PER Nuclear and Cytoplasmic Extraction kit as per the

manufacturer's protocol, with around 6 million cells per 10-cm plate to generate 1 µg/µl protein lysates. Protein quantification was done by Pierce BCA Assay (23225, Life Technologies).

For experiments assessing BiP protein levels, wild-type versus clonal *Fitm2*Δ isogenic Renca cells were used. A total of 0.5×10^6 cells were seeded into 10-cm plates and cultured for 24 h, followed by treatment with increasing doses of tunicamycin (Abcam, ab120296) or IFNγ (100 ng/ml) for 24 or 72 h, respectively. Cells were washed once with 1×PBS and collected in 1× RIPA buffer (BP-115, Boston Bioproducts) containing phosphatase and protease inhibitor cocktail (5872S, Cell Signaling Technologies). Cell lysates were briefly sonicated and subsequently cleared by centrifugation at 14,000 rpm for 10 min at 4 °C. Protein quantification was done by Pierce BCA Assay (23225, Life Technologies).

For immunoblotting analysis, lysates were loaded onto precast SDS–PAGE gels (5671093, Bio-Rad) and subsequently transferred onto nitrocellulose membrane for detection. All primary antibodies were probed overnight at 4 °C, and membranes were washed with TBST and incubated with appropriate secondary antibodies for 1 h. Subsequently membranes were washed with TBST and visualized using the Odyssey imaging system (LI-COR).

The primary antibodies used were ATG12 (20H24L24) (701684, Invitrogen, 1:250), LC3b (ab51520, Abcam, 1:3,000), NF-κB p65 (D14E12) (8242, Cell Signalling, 1:1,000), phospho-NF-κB p65 (Ser536) (93H1) (3033, Cell Signalling, 1:1,000), IκBα (9242, Cell Signalling, 1:1,000), NRF2/NFE2L2 (D1Z9C) (12721, Cell Signalling, 1:1,000), SQSTM1/P62 (5114, Cell Signalling, 1:1,000), alpha tubulin (T6074, Sigma Millipore, 1:5,000), Histone H3 (9715, Cell Signalling, 1:1,000), BiP (C50B12, Cell Signalling, 1:1,000), GAPDH (2118S, Cell Signalling, 1:5,000). Secondary antibodies used were IRDye 680RD donkey anti-rabbit (926–68073, LI-COR, 1:5,000) and IRDye 800CW donkey anti-mouse (926–32212, LI-COR, 1:5,000).

Raw data for western Blots shown in Extended Data Figs. 6e, 9c are provided in the Supplementary Information.

Flow cytometry

For the analysis of MHC-I and MHC-I bound to OVA on B16–Ova, cells were treated (or not) with 10 nM of mouse recombinant IFNγ (78021.2, StemCell) for 96 h, lifted from the culture plates using trypsin EDTA and washed once in FACS buffer (PBS containing 5% FBS). After washing, cells were stained at 4 °C for 30 min in FACS buffer containing MHC-I (anti mouse MHC-I (H-2 kb) EFluor450 at 1:200, clone AF6-88.5.5.3, Ebiosciences) and MHC-I bound to OVA (anti mouse OVA 257-264 peptide bound to H2kb PE at 1:100, clone 25-D1.16, Ebiosciences) antibodies. After staining, cells were washed in FACS buffer, and resuspended in FACS buffer containing 1:500 of ToPro-3 for live and dead discrimination (T3606, Invitrogen). Samples were run in triplicate using a LSR Fortessa instrument (BD Biosciences) equipped with 5 lasers and a HTS. FACSDIVA v.6 software was used during data acquisition. Median fluorescent intensities (MFI) were calculated using FlowJo software (FlowJo v.10.6.1). The FACS gating strategy is provided in the Supplementary Information.

Lentivirus production

Lentivirus was produced via co-transfection of packaging (psPAX2, Addgene 12260), envelope (pMD2.G, Addgene 12259) and transfer plasmids into 293T cells using the X-treme Gene 9 transfection reagent (Roche). Sixteen hours after transfection, 293T culture medium was changed to viral collection medium consisting of DMEM supplemented with 1% BSA and 1% penicillin–streptomycin, and cells were incubated for 36–48 h. Virus-containing medium was collected and centrifuged at 2,000 rpm to remove cell debris and then aliquoted and stored at −80 °C.

For mTKO genome-wide and validation library virus production, the MOI was determined by functional titering for each cell line screened by comparing the fraction of surviving cells in transduced versus untransduced populations following puromycin selection.

TCGA analysis

RNA-seq V2 data from the TCGA PanCancer Atlas were retrieved from the cBioPortal using the cgdsr R package v.1.3.0 (10,071 tumour samples across 32 tumour types; 6,935 used for analysis) and National Cancer Institute (NCI) Genomic Data Commons (GDC) using TCGAbiolinks R package v.2.16.0 (9,353 tumour samples; 5,708 used for analysis). Tumour gene expression data were extracted from these datasets for 182 core cancer-intrinsic CTL-evasion genes; representative random gene sets (negative control); and expression data for *GZMA* and *PRF1* to calculate the cytolytic index, as previously defined[5]. Corresponding data for other immune response surrogates (immune characteristics data, hERV expression, innate anti-PD1 resistance or IPRES signature data) were obtained from previous studies[4,22,23]. Core cancer-intrinsic CTL-evasion genes were stratified by suppressor or sensitizer status and pairwise partial Spearman correlations (pcor.test function; ppcor R package v1.1) were performed between the expression levels of each gene set and immune response surrogates, while controlling for the confounding effects of tumour purity. Tumour purity data were obtained from a previous study[41]. Unbiased hierarchically clustered heat maps were produced using the gplots R package

In vivo *Adar* validation

Tumours were established by subcutaneously injecting 100 µl of B16F10 cells stably expressing inducible iShADAR1 (hairpin sequence: GGAGA AGATCTGTGACTATCT) at a concentration of 2.5×10^5 cells per mouse in the right flank of each mouse. Similarly, tumours in NSG mice were established by subcutaneously injecting 100 µl of cells at a concentration of 5.0×10^4 cells per mouse also into the right flank of each mouse. All cell lines were prepared for implantation by resuspending cells in a 1-to-1 ratio of PBS and Matrigel. Upon establishment of tumours (100–150 mm^3), mice were randomized into two groups: vehicle or doxycycline treatment. No power calculation for sample size was performed. The doxycycline treatment group was placed on an ad libitum diet of irradiated Prolab RMH 3000 (standard rodent diet) with 500 ppm (500 mg kg^{-1}) doxycycline, formulated by Testdiets (https://www.labdiet.com/) for the remainder of the experiment. Tumour volume was measured three times per week by caliper, and volume was calculated using the formula $0.5 \times W^2 \times L$ with the results presented as mean and standard error of mean (s.e.m.). Tumour volume measurements were not blinded. A tumour size limit of 2,000 mm^3 was used as a humane end point. At the end of the study, mice were euthanized by CO_2 inhalation.

Experimental set-up for in vivo screen

Cas9-expressing EMT6–HA cells were infected in triplicate pools with the mVal library at an MOI of around 0.3 at around 7,000× representation. Cells were propagated in vitro with serial cell pellets and maintained at a representation of around 2,000×). On T7, 2.5×10^6 cells within each replicate were pooled and injected subcutaneously into the right hindflank of NCG ($n = 90$) or BALB/c ($n = 107$) mice. Sample size was chosen to ensure high library coverage (more than 5,000×) assuming a low cancer cell engraftment success rate (around 5%). Cells from each replicate were distributed evenly amongst mice. For each replicate, in vitro cell populations at were maintained at around 2,000× representation. At each passage, cell pellets were collected at more than 500-fold library coverage for genomic DNA extraction, starting on day 0 post-selection, with T6 representing the preimplantation samples.

Mice were monitored twice weekly for tumour size with calipers. Once tumours became obviously palpable (around 7 days after implantation), a cohort of NSG and BALB/c mice were euthanized (around 30 mice each), then tumours were collected and flash-frozen in liquid nitrogen following manual surgical removal to establish an early time point. The remaining tumours were monitored over a period of 5 weeks,

with tumours being collected after displaying an obvious pattern of persistent growth. All tumours collected after the first round (that is, the early time point) were categorized into the late time point. A total of 17 early and 72 late tumours were collected from NCG mice, whereas 28 early and 61 late tumours were collected from BALB/c mice.

Sample processing and construction of sequencing library for in vivo screen

For each tumour sample, around 100 mg of tumour tissue was excised and minced into small pieces using a razor blade. Genomic DNA was purified from minced tissues using the Promega Wizard Genomic Purification kit according to the manufacturer's instructions. For each tumour sample, the gRNA cassette was amplified directly from 1 µg of genomic DNA using primers containing Illumina TruSeq adaptors with i5 and i7 barcodes. The resulting sequencing libraries were pooled and gel-purified. For samples in the in vitro control arm, the gRNA cassette was amplified from 14 µg of genomic DNA. All sequencing libraries were sequenced on the Illumina NextSeq 550 instrument.

Analysis of in vivo screen results

Identifying in vivo essential genes. In vivo essential genes were identified using the early time point under the assumption that gRNA targeting essential genes will be underrepresented relative to the remaining gRNA in the library. Individual genes were ranked according to total gRNA counts within each mouse sample and used to construct gene-level rank distributions. For each gene, NCG and BALB/c rank distributions were pooled and hierarchically clustered using Jensen-Shannon divergence as the distance metric. Discrete clusters were then defined using an adaptive branch pruning method[42]. Putative essential gene clusters were then defined as those rank distributions that were positively skewed and had <20th percentile median rank. From this list of putative essential genes (that is, genes belonging to pink and turquoise clusters) gene-level gRNA rank distributions were compared between NCG and BALB/c mice, and those that were consistent (that is, FDR < 0.001, two-sided rank-sum test) were classified as in vivo essential genes. To construct a rank plot for in vivo essentials, gene ranks were compared to targeting controls by Wilcoxon rank-sum test and ranked according to FDR. The list of in vivo essential genes was compared to in vitro EMT6 essential genes (BF > 50) with a Venn diagram.

Quantifying strain-dependent in vivo effects. To quantify strain-dependent differences in the EMT6 in vivo screen, individual genes were ranked according to total gRNA counts within each mouse sample, and time- and strain-matched gene ranks were aggregated as median ranks. From these genes, all in vivo essential genes were omitted. For each time point, pairwise-gene rank comparison between BALB/c and NCG mice was performed using two-sided Wilcoxon rank-sum test, and *P* values were adjusted using the Benjamini–Hochberg correction. Log-transformed *P* values were signed according to the sign of BALB/c−NCG rank differences and used to construct rank plots.

A gRNA-level analysis of differential fold change (FC) between BALB/c and NCG was also conducted using the formula mean ($FC_{BALB/c}$) − mean(FC_{NCG}), where $FC_{BALB/c} = \log_2$(BALB/c read counts at early or late time points) − $\log_2$(BALB/c T6-normalized T0 read counts), and $FC_{NCG} = \log_2$(NCG read counts at early or late time points) − $\log_2$(NCG T6-normalized T0 read counts). For each gRNA in the mTKO library, T6-normalized T0 read counts were calculated by subtracting the T0 read counts for a given in vivo tumour sample by the preimplantation level obtained in vitro (that is, T6 time point), and subsequently normalizing to read depth. Gene-level statistics were generated by comparing the difference in mean FC of each gRNA across time-point-matched (that is, early versus late) BALB/c versus NCG tumour samples.

Transmission electron microscopy

For electron microscopy sample preparation, Renca wild-type, *Fitm2*Δ and *Atg12*Δ cells were cultured to around 80% confluency and fixed in 2.5% glutaraldehyde (Sigma Aldrich) in 0.1 M sodium cacodylate (pH 7.4, Sigma Aldrich) for 3 h at room temperature and then shifted to 4 °C overnight. For primary washing, glutaraldehyde and sodium cacodylate were removed from samples, followed by three wash steps for 10 min each using 0.1 M sodium cacodylate rinse buffer (prepared using sodium cacodylate trihydrate diluted in ultrapure water, Sigma Aldrich) at room temperature. The samples were post-fixed with 1% osmium tetroxide (Sigma Aldrich) in 0.1 M sodium cacodylate buffer for 90 min at room temperature, followed by three wash steps for 10 min each using 0.1 M sodium cacodylate rinse buffer. The samples were then dehydrated using a graded series of ethanol in distilled water (50%, 70%, 90%, 100%) for 15 min twice at each step. Next, the samples were infiltrated with 50% Quetol651 epoxy resin (Thermo Fisher Scientific) for 2 h at room temperature then shifted to 4 °C overnight. Next day, the samples were treated with 100% Quetol651 epoxy resin for 4 h then embedded in fresh resin and polymerized in a 60 °C oven for 48 h. After complete polymerization, the samples were sectioned on a Leica UC7 Ultramicrotome diamond knife to 50–70-nm thickness. Finally, the samples were stained with 2% uranyl acetate (Thermo Fisher Scientific) for 20 min then rinsed six times with distilled water and stained in 0.1% aqueous lead citrate (Thermo Fisher Scientific) for 20 min. This was followed by a final rinse using distilled water and then samples were air-dried. Sections were observed under a FEI Tecnai 20 TEM at an accelerating voltage of 80 kV. Images were acquired using TEM Imaging and Analysis (TIA) software (v.4.0).

Statistical analysis

For all experiments, the number of technical and/or biological replicates is provided in the figure legends or text. Microsoft Excel (v.16.16.12) was used to organize data into tables. In all cases $^{****}P < 0.0001$, $^{***}P < 0.001$, $^{**}P < 0.01$, $^{*}P < 0.05$. Statistical analyses were performed using GraphPad Prism v.8.2.1 (GraphPad) or the R language (v.3.6.1) programming environment using RStudio (v.1.1.456).

Reporting summary

Further information on research design is available in the Nature Research Reporting Summary linked to this paper.

Data availability

The datasets generated and analysed in this study are included in the manuscript. The raw FASTQ files for the sequencing data are available upon request and have also been deposited as a superset to the GEO (https://www.ncbi.nlm.nih.gov/geo/) with accession number GSE149936. Descriptions of the analyses, tools and algorithms are provided in the Methods and Reporting Summary. Source data are provided with this paper.

Code availability

Custom code for generating the qNormZ scores, differential NormZ scores, essential gene clustering and gene ranks will be available on GitHub (https://github.com/NMikolajewicz/Lawson2020).

31. Diebold, S. S., Cotten, M., Koch, N. & Zenke, M. MHC class II presentation of endogenously expressed antigens by transfected dendritic cells. *Gene Ther.* **8**, 487–493 (2001).
32. Mair, B. et al. Essential gene profiles for human pluripotent stem cells identify uncharacterized genes and substrate dependencies. *Cell Rep.* **27**, 599–615 (2019).
33. Colic, M. et al. Identifying chemogenetic interactions from CRISPR screens with drugZ. *Genome Med.* **11**, 52 (2019).
34. Subramanian, A. et al. Gene set enrichment analysis: a knowledge-based approach for interpreting genome-wide expression profiles. *Proc. Natl Acad. Sci. USA* **102**, 15545–15550 (2005).

35. Michailidou, K. et al. Association analysis identifies 65 new breast cancer risk loci. *Nature* **551**, 92–94 (2017).
36. Lee, I., Date, S. V., Adai, A. T. & Marcotte, E. M. A probabilistic functional network of yeast genes. *Science* **306**, 1555–1558 (2004).
37. Kanehisa, M., Furumichi, M., Tanabe, M., Sato, Y. & Morishima, K. KEGG: new perspectives on genomes, pathways, diseases and drugs. *Nucleic Acids Res.* **45**, D353–D361 (2017).
38. Giurgiu, M. et al. CORUM: the comprehensive resource of mammalian protein complexes-2019. *Nucleic Acids Res.* **47**, D559–D563 (2019).
39. Dobin, A. et al. STAR: ultrafast universal RNA-seq aligner. *Bioinformatics* **29**, 15–21 (2013).
40. Seki, A. & Rutz, S. Optimized RNP transfection for highly efficient CRISPR/Cas9-mediated gene knockout in primary T cells. *J. Exp. Med.* **215**, 985–997 (2018).
41. Yoshihara, K. et al. Inferring tumour purity and stromal and immune cell admixture from expression data. *Nat. Commun.* **4**, 2612 (2013).
42. Langfelder, P., Zhang, B. & Horvath, S. Defining clusters from a hierarchical cluster tree: the Dynamic Tree Cut package for R. *Bioinformatics* **24**, 719–720 (2008).

Acknowledgements We thank all members of the J.M. laboratory; T. Griffith for discussions; and E. Miazima for assistance with molecular biology experiments. K.A.L. was supported by a Vanier Canada Graduate Scholarship and Studentship award from the Kidney Cancer Research Network of Canada; E.K. was supported by the Cancer Prevention Research Institute of Texas (CPRIT) grant RR160032; and T.H. is a CPRIT Scholar in Cancer Research and is supported by NIGMS grant R35GM130119 and MD Anderson Cancer Center Support Grant P30 CA016672. This research was funded by grants from the Ontario Institute of Cancer Research (J.M.), an industry sponsored grant from Agios Pharmaceuticals (J.M.) and the Canadian Institutes for Health Research (MOP-142375 to J.M.). J.M. holds a Canadian Research Chair in Functional Genomics.

Author contributions Conceptualization and design of the study: K.A.L. and J.M. Experimental investigation: K.A.L., C.M.S., X.Z., R.A., J.J.C., Y.Y., A.A.Z., J.A.K., D.M.S., C.J.S., V.D.J., L.T., R.S., J.E.G., S.M., Q.H., E.A.F., A.H., R.C., D.T., J.W., R.L., A.H.Y.T., M.A., K.S.C., H.H., X.W. and P.M. Data analysis: K.A.L., C.M.S., E.K., R.A., N.M., Z.P.F., S.H., G.B., P.M., C.R., K.R.B., T.H. and J.M. Writing (original draft): K.A.L. and J.M. Writing (reviewing and editing): K.A.L. and J.M., with input from the other authors. Supervision: J.M., K.A.L., C.M.S., C.K., J.H.B., T.H., G.A.K., L.A., G.A.S. and A.F. Funding acquisition: J.M., K.A.L., L.A. and A.F.

Competing interests C.M.S., Z.P.F., J.A.K., S.M., D.M.S., C.J.S., V.D.J., L.T., R.S., J.E.G., G.A.S., G.A.K. and C.K. are employees of and have ownership interest in Agios Pharmaceuticals. This project was funded in part through a sponsored research agreement awarded to J.M. from Agios Pharmaceuticals. J.M. is a shareholder in Northern Biologics and Pionyr Immunotherapeutics, and is an advisor and shareholder of Century Therapeutics and Aelian Biotechnology. A.F. has received honoraria from Amgen, Abbvie, Janssen, Astellas, Sanofi, Bayer and TerSera (advisory boards and invited speakers), and research funds through a sponsored research agreement with Celsius Therapeutics. The remaining authors declare no competing interests.

Additional information

Supplementary information is available for this paper at https://doi.org/10.1038/s41586-020-2746-2.

Correspondence and requests for materials should be addressed to J.M.

Peer review information *Nature* thanks William Haining and the other, anonymous, reviewer(s) for their contribution to the peer review of this work.

Reprints and permissions information is available at http://www.nature.com/reprints.

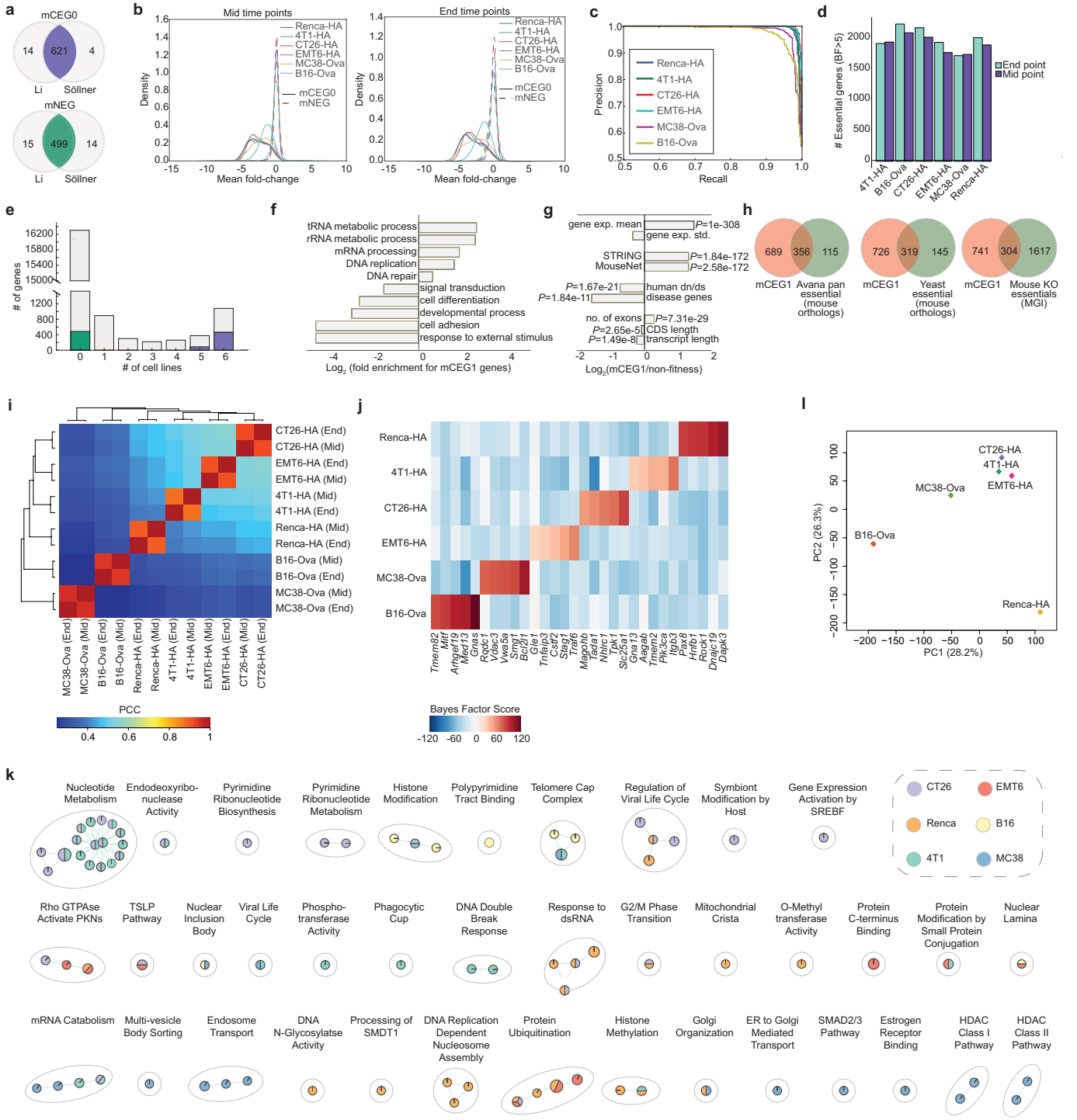

Extended Data Fig. 1 | Assessment of core and context-specific mouse fitness genes with the mTKO library. a, Overlap of mouse core essential genes (mCEG0) and non-essential genes (mNEG), indicated in purple and green, respectively, that are orthologous to the corresponding human gene sets, as determined from either the Li or Söllner datasets. **b**, Mean fold change distributions of core essential genes (mCEG0) or non-essential genes (mNEG0) across the indicated screens at mid and end time points, where fold change is calculated as $\log_2$(normalized read counts from early or late time points) – $\log_2$(normalized T0 read counts). **c**, Precision-recall plots derived using the reference essential (mCEG0) and non-essential (mNEG) gene sets for the indicated screens. **d**, Number of genes with BF >5 at mid and late time points across all screens. **e**, Number of essential genes (BF >5) across the six cell lines assayed with the mTKO library. Genes in the mCEG0 or mNEG gene sets described in part A are indicated as purple or green stacks in their respective bars. **f**, Selected biological processes enriched or depleted in the mTKO core essential genes as defined by the mCEG1 gene set (FDR <5%). **g**, General biological properties of the mTKO core essential genes, plotted as fold-change of the mCEG1 gene set relative to reference non-essential genes. One sided Fisher's exact test was used for calculating *P* values of disease genes and two-sample Kolmogorov-Smirmov test for other features. **h**, Overlap of mCEG1 genes with other reference essential gene lists from human, yeast and whole-organism mouse knockout studies. **i**, Correlation and unsupervised clustering of genotype-specific essential gene profiles across all cell lines and time points. **j**, BF scores for top 5 genotype-specific essential genes for each cell line. **k**, Pathways enriched at FDR < 5% uniquely in fewer than three cell lines, as identified by GSEA analysis on rank-ordered essential genes from each screen. **l**, Principal component analysis of transcriptomic data for replicate samples from each cell line.

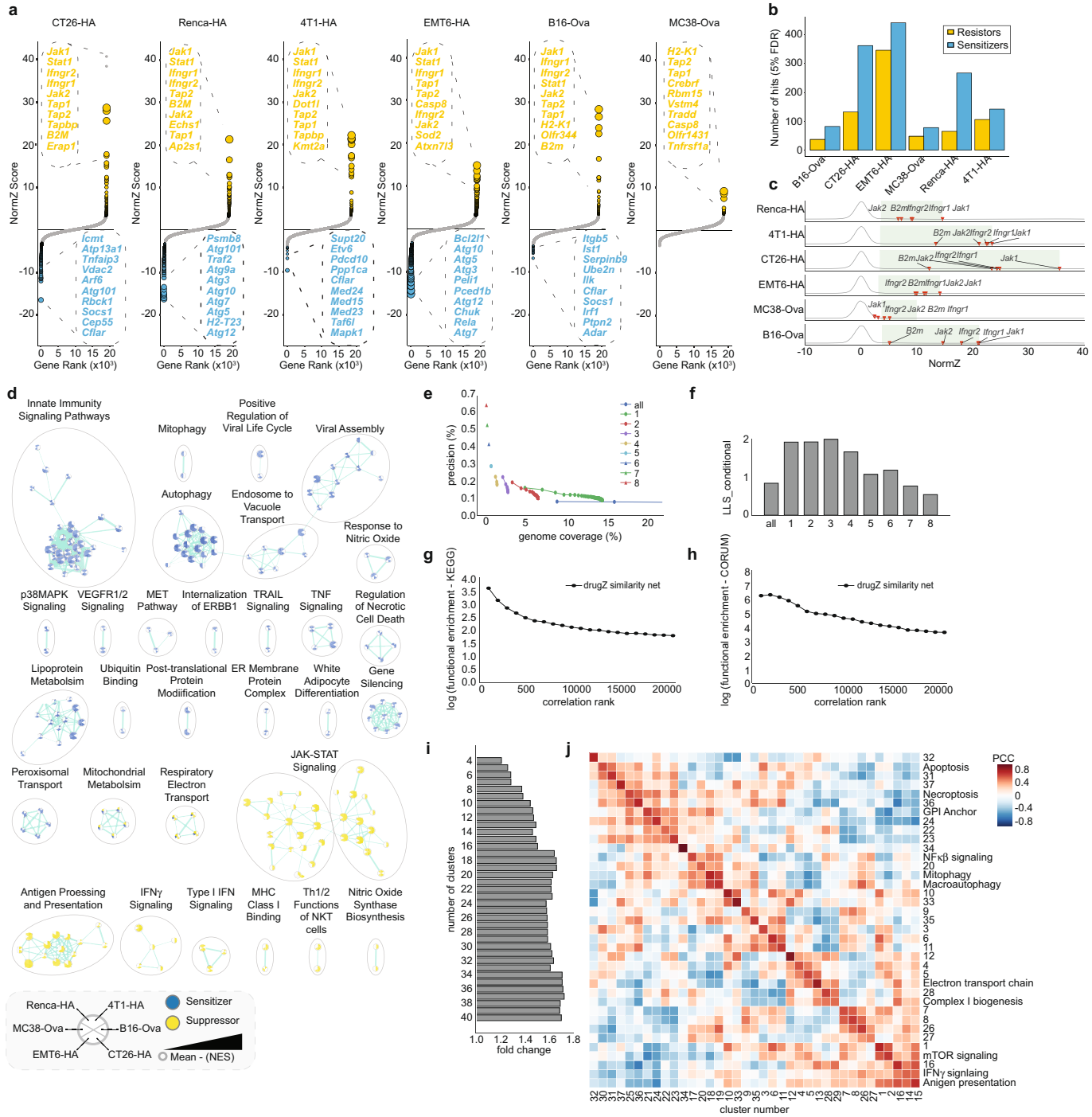

Extended Data Fig. 2 | Supplementary analysis of cancer-intrinsic CTL-evasion genes. a, Rank-ordered NormZ scores at the end time point for all six CTL killing screens. Hits at FDR < 5% are highlighted in yellow (resistor genes) and blue (sensitizer genes). The top 10 resistor and sensitizer genes are indicated. Dots size inversely scaled by FDR. **b**, Number of drugZ sensitizing and suppressor hits at FDR <5% for each screen. **c**, Gene-level NormZ scores for *Jak1*, *Jak2*, *B2m*, *Ifngr1* and *Ifngr2* across all screens. Green box highlights FDR < 5% window for suppressor hits. **d**, Enrichment map showing resistance and sensitization pathways enriched in three or more cell lines using GSEA (FDR < 5%). **e**, Precision (that is, functional enrichment) versus genome coverage for gene pairs included in the co-similarity network at various hit thresholds (that is, number of times a gene is a hit at FDR < 5%). Precision is defined as the number of gene pairs co-annotated to a pathway for a given filtered dataset divided by the total number of co-annotated gene pairs in the Bader lab pathway database. Genome coverage is defined as the number of genes included in the filtered dataset over the total number of genes in the mouse genome. For each plotted dataset, consecutive circles represent 1,000 gene pairs. Triangles are shown for datasets with fewer than 1,000 gene pairs. For "all data" dataset, only the first 3,000 gene pairs are shown. **f**, The conditional log-likelihood score (LLS) of the first 1,000 gene pairs for each derived network at a given hit threshold. **g**, **h**, Enrichment for co-annotated gene pairs included in the co-similarity network derived from genes significant in at least three screens and time points using the KEGG and CORUM databases. **i**, Functional enrichment for co-annotated gene pairs within clusters across various cluster number thresholds. **j**, Correlation matrix depicting the mean Pearson correlation coefficient of all pairwise cluster combinations. Mean PCC were calculated across all individual gene pairs PCC in a given cluster. Representative pathways enriched in a cluster are shown at right (FDR < 1%). If no pathways were significantly enriched, the cluster number is displayed.

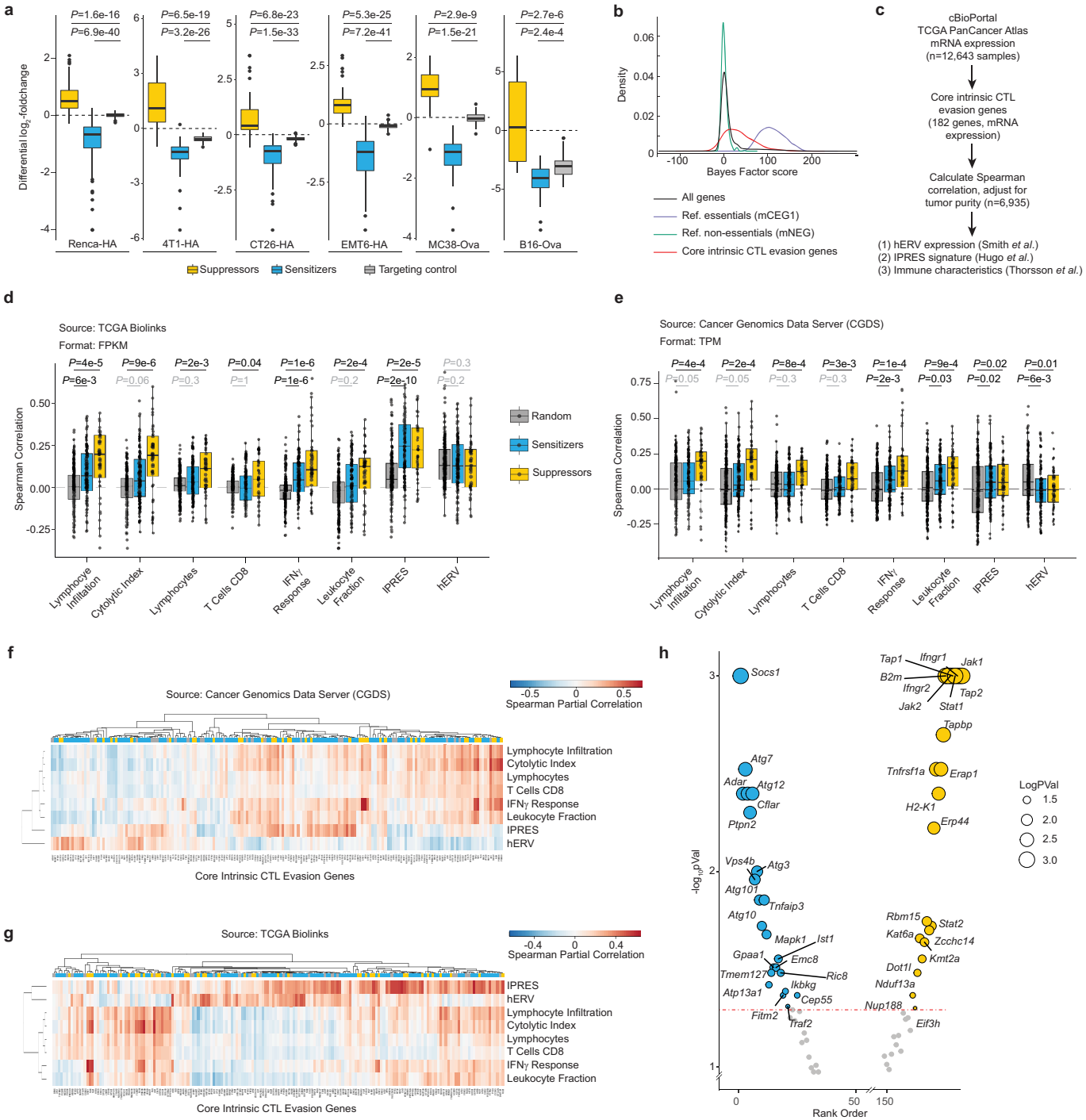

Extended Data Fig. 3 | See next page for caption.

Extended Data Fig. 3 | Supplementary analysis of core cancer-intrinsic CTL-evasion genes. a, Differential log_2-fold change results for secondary validation screens. CTL killing screens in six cell lines using a mini sgRNA library targeting all 182 core cancer-intrinsic CTL-evasion genes. Boxplots for major groups of genes in the validation library including resistor genes ($n = 70$), sensitizer genes ($n = 140$) and targeting controls ($n = 182$). Boxes show the interquartile range (IQR), with the median indicated by a line. The whiskers extend to the quartile ±1.5 × IQR. Statistical significance was determined by a two-sided Wilcoxon rank sum test between targeting control and resistor or sensitizer groups. **b**, Distribution of gene essentiality scores (Bayes Factors) for core cancer-intrinsic CTL evasion genes, reference essential (mCEG1), non-essential (mNEG) or all genes targeted by the mTKO library. **c**, Workflow for TCGA analysis. **d**, **e**, Spearman correlation coefficients between core cancer-intrinsic CTL-evasion genes and immune response surrogates using RNA-seq data from Pan-Cancer TCGA cohort samples ($n = 5{,}708$ and $n = 6{,}935$ for data retrieved with TCGA BioLinks (**d**) and Cancer Genomics Data Server (**e**), respectively). Sensitizers ($n = 110$ (TCGA Biolinks), $n = 109$ [CGDR]) and suppressors ($n = 40$ (TCGA Biolinks), $n = 40$ [CGDR]) were compared to random genes ($n = 177$ (TCGA Biolinks), $n = 176$ (CGDR)) using two-sided Wilcoxon rank-sum test and *P*-values were adjusted using Benjamini-Hochberg correction, with $P < 0.05$ significance threshold. 27 genes were omitted from comparison owing to varying sensitizer/suppressor classifications across cancer lines, and 5 (TCGA Biolinks) or 6 (CGDR) omitted owing to incomplete data. Data points are gene-level correlations and boxplots show median (50th percentile; middle line), interquartile range (IQR; 25th to 75th percentiles; box edges) and distribution tails (± 1.5 × IQR; whiskers). **f**, **g**, Heat map of Spearman correlation coefficients between mRNA expression of each core intrinsic CTL-evasion gene and various immune response characteristics[4,22,23]. Sensitizers (blue) and suppressors (yellow) are colour-coded accordingly. **f**, TCGA data obtained from Cancer Genomics Data Server($n = 6{,}935$ samples); **g**, data from TCGA BioLinks ($n = 5{,}708$ samples). **h**, Plot of rank-summarized *P*-values and NormZ scores for strongest resistor and sensitizing core cancer-intrinsic CTL killing genes across all screens. Genes with $-\log_{10}$(Rank pVal) >3 plotted at 3 for display purpose.

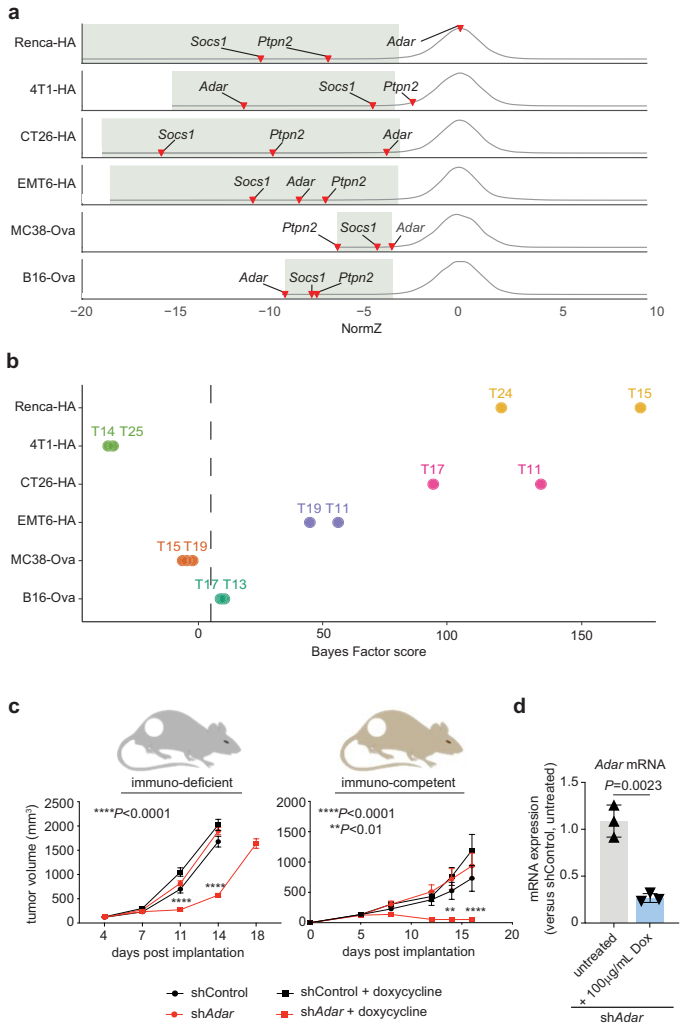

Extended Data Fig. 4 | Additional data for *Adar*. **a**, Distribution of gene-level NormZ scores for all six CTL killing screens. Well-characterized core CTL killing genes including *Socs1*, *Ptpn2* and *Adar* are indicated for each screen, and green boxes highlight the FDR <5% window for sensitizing hits. **b**, BF values for *Adar* across each cell line. **c**, Tumour burden in B16F10 bearing immunodeficient (left) or immunocompetent (right) mice following dox-induced shRNA-mediated knockdown of *Adar* (red) or control (black) ($n = 10$ mice per group). Error bars, s.e.m. Dox-treated mice are indicated by squares and non-treated controls are indicated by circles. **d**, qPCR analyses of *Adar* mRNA levels following dox-induced shRNA knockdown, as quantified by Taqman assay. Error bars, s.d.; technical triplicates of one experiment. Two-way ANOVA with Fisher's LSD comparison.

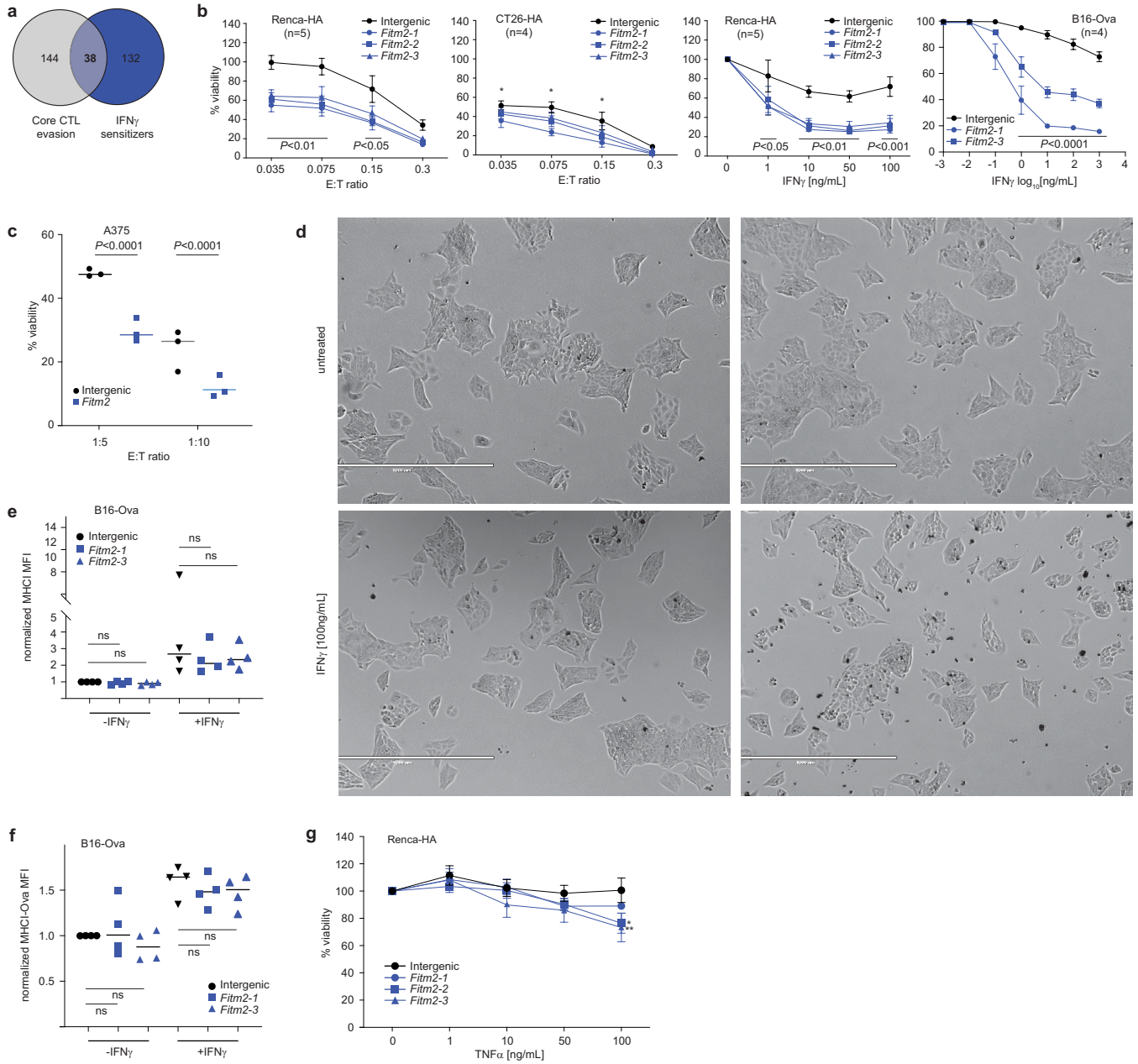

Extended Data Fig. 5 | Phenotypic effects following perturbation of *Fitm2*. **a**, Overlap of core intrinsic CTL-evasion genes and hits from the Renca IFNγ screen. **b**, Per cent viability of *Fitm2* or intergenic gRNA-transduced Renca-HA, B16-Ova or CT26-HA cells treated with escalating doses of antigen-specific (CL4) T cells or IFNγ. Error bars equal s.e.m. of indicated number (*n*) of independent experiments. For CT26HA panel, * denotes *Fitm2-1* *P*-value <0.05. *P*-values determined by Two-way ANOVA with Fisher's LSD comparison. **c**, Per cent viability of *Fitm2* or intergenic gRNA-transduced human A375 cells treated with escalating doses of antigen-specific (WT-1) T cells. Data representative of 3 independent experiments, with line highlighting mean effect. *P* values determined by two-way ANOVA with Fisher's LSD comparison. **d**, Microscopic views of *Fitm2* (right panels) or intergenic (left panels) gRNA-transduced Renca cells after 72 h of IFNγ treatment shown (lower panels). Untreated control cells are shown in the top panels. Data represent a single experiment. **e**, Expression of surface MHC-I by flow cytometry for B16-Ova cells transduced with *Fitm2* or intergenic gRNAs and treated with IFNγ. Data representative of 4 independent experiments, with line highlighting mean effect. *P* values determined by two-way ANOVA with Fisher's LSD comparison. **f**, Expression of surface MHC-I/Ova(SIINFEKL) by flow cytometry for B16-Ova cells transduced with *Fitm2* or intergenic gRNAs and treated with IFNγ. Data representative of 4 independent experiments, with line highlighting mean effect. *P* values determined by two-way ANOVA with Fisher's LSD comparison. **g**, Per cent viability of *Fitm2* or intergenic gRNA-transduced RencaHA cells treated with increasing doses of TNF for 72 h. Errors bars equal s.e.m. of 5 independent experiments. For 100 ng ml^{-1} dose, * or ** denote *P* values <0.05 and <0.01, respectively, for *Fitm2*-2 and *Fitm2*-3, respectively. *P* values determined by two-way ANOVA with Fisher's LSD comparison. Note: overlap of data for intergenic control with Fig. 3b.

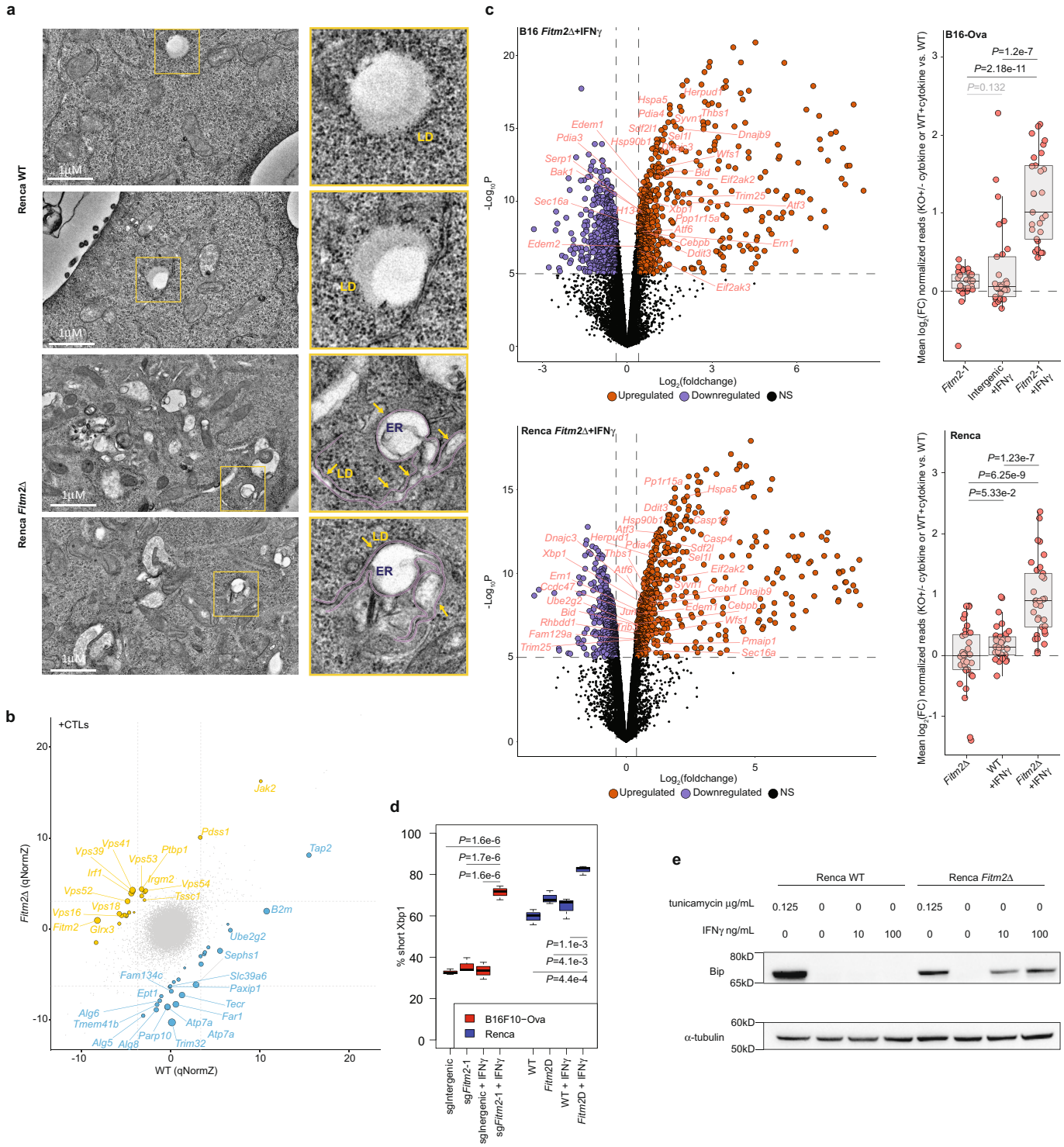

Extended Data Fig. 6 | See next page for caption.

Extended Data Fig. 6 | Additional data for *Fitm2*. **a**, TEM photo showing defective lipid droplet budding in Renca *Fitm2*Δ cells compared to WT cells. Data represents a single experiment. **b**, Sectored scatter plots of gene-level quantile normalized NormZ scores (qNormZ) from WT and *Fitm2*Δ cells propagated under CTL selection pressure. Significant negative and positive GIs (FDR < 5%) are coloured blue and yellow, respectively. Dashed line reflects median NormZ of GIs. **c**, Differential gene expression between IFNγ–treated (48 h) WT and *Fitm2*Δ B16–Ova cells (top) or Renca (bottom) cells highlighting downregulated (purple; B16 $n = 589$; Renca $n = 668$) and upregulated (orange; B16 $n = 716$; Renca $n = 765$) genes (FDR < 5%). Representative genes for the GO:BP ER stress pathway (GO:0034976) are labelled (B16 $n = 31$; Renca $n = 40$). For B16, polyclonal KO populations were used by transducing cells with sg*Fitm2* or sgIntergenic (control) guide RNAs. Clonal *Fitm2*Δ versus WT cells used for Renca. Side box plots display mean fold change (where fold change = $\log_2$(KO or WT read counts ± cytokine) − $\log_2$(WT read counts)) of ER stress pathway genes between *Fitm2*Δ, IFNγ treated or *Fitm2*Δ + IFNγ treatment conditions relative to WT cells. Boxes show the interquartile range (IQR, 25th to 75th percentile), with the median indicated by a line. The whiskers extend to the quartile ± 1.5 × IQR. Data representative of 3 independent biological replicates, and statistical significance was determined by a two-sided Student's *t*-test between each treatment condition group. **d**, *Xbp1* splicing in B16–Ova and Renca cells transduced with intergenic versus *Fitm2* sgRNAs and treated with IFNγ for 48 h. Boxes show the interquartile range (IQR, 25th to 75th percentile), with the median indicated by a line. The whiskers extend to the quartile ± 1.5 × IQR. Data representative of 3 independent biological replicates, and comparisons were performed using pairwise two-sided *t*-tests with Holm's multiple testing correction. **e**, Western blot of BiP protein in Renca WT and *Fitm2Δ* cells treated with escalating does of tunicamycin or IFNγ. Data representative of three independent experiments.

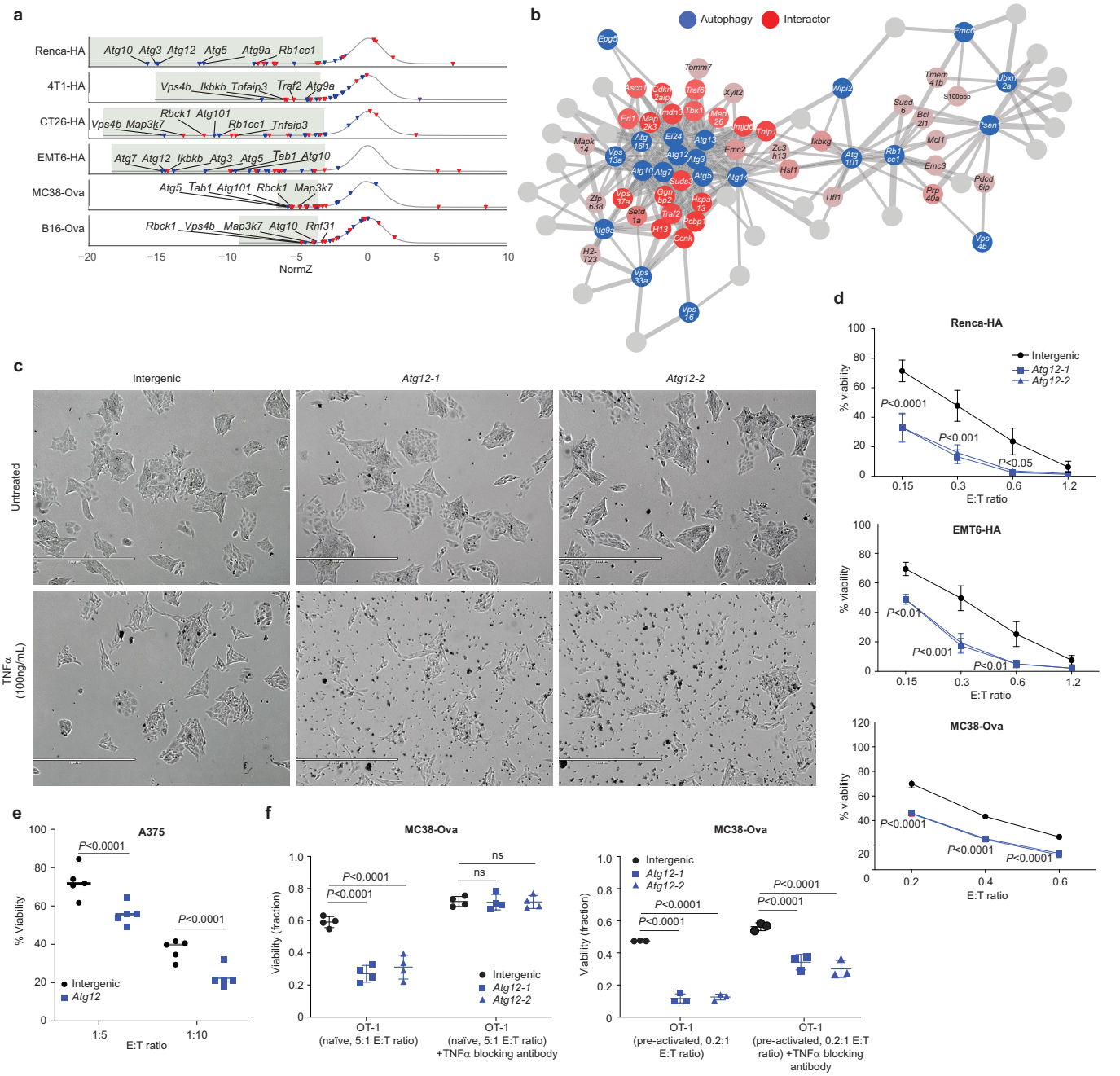

Extended Data Fig. 7 | Phenotypic effects after perturbation of *Atg12*. **a**, Distribution of gene-level NormZ scores for all six CTL killing screens. Core intrinsic CTL-evasion genes belonging to the autophagy (blue) and NF-κβ (red) pathways are indicated for each screen, and green boxes highlight the FDR < 5% window for sensitizing hits. **b**, Genetic co-similarity subnetwork showing genes (that is, interactors; red) with NormZ score profiles highly correlated to autophagy pathway genes (blue) across all screens at FDR < 5%. **c**, Microscopic views of Renca–HA cells transduced with sgRNAs against intergenic control sites or *Atg12* and treated with TNF for 72 h. Data represents a single experiment. **d**, Per cent viability of *Atg12* or intergenic gRNA-transduced cancer cells treated with escalating doses of antigen-specific T cells for 24 h. For all plots, error bars are s.e.m. For Renca–HA and EMT6–HA, data represent five independent experiments. For MC38, data represent one experiment with four technical replicates. *P* values determined by two-way ANOVA with Fisher's LSD comparison. Note: overlap of data for Renca–HA with Fig. 3c, plotted separately here. **e**, Per cent viability of *Atg12* or intergenic gRNA-transduced human A375 cells treated with increasing doses of antigen-specific (WT-1) T cells. Data representative of 5 independent experiments, with line highlighting mean effect. *P* values determined by two-way ANOVA with Fisher's LSD comparison. **f**, Viability of MC38-Ova cells transduced with gRNAs targeting *Atg12* or intergenic control sites and treated with naive (left) or preactivated (right) OT-1 T cells with or without anti-TNF blocking antibodies. Error bars are s.e.m. of a single experiment with at least four technical replicates. *P* values determined by two-way ANOVA with Fisher's LSD comparison.

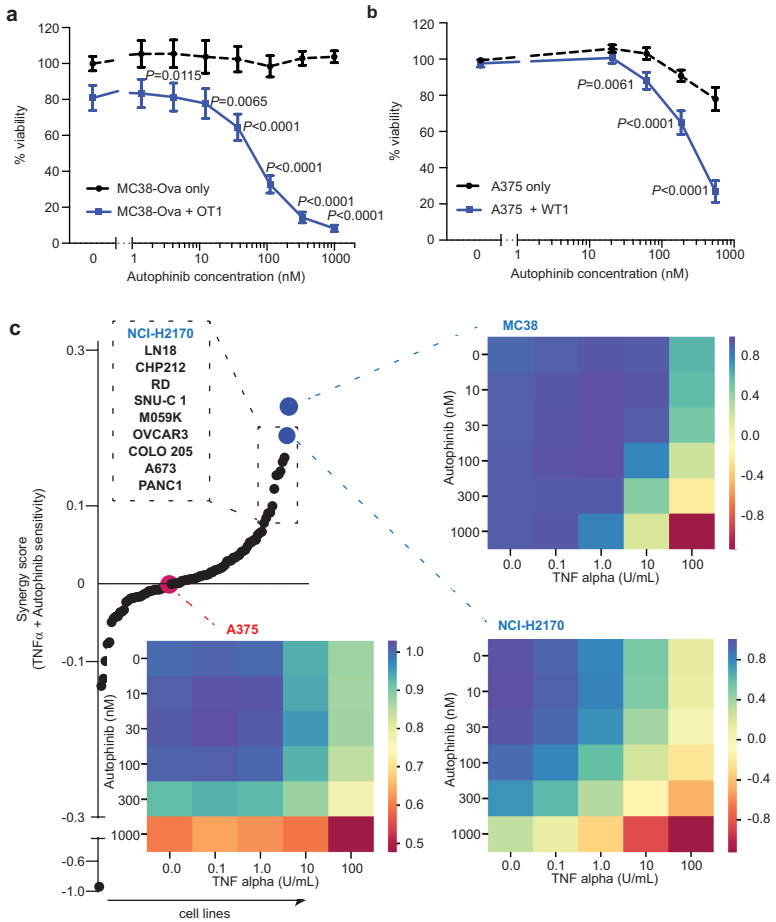

Extended Data Fig. 8 | Chemical inhibition of autophagy synergizes with TNF treatment in a subset of human cancer cell lines. Viability of MC38-OVA (**a**) and A375 (**b**) cells treated with antigen-specific T cells (OT-I at 5:1 and WT1 at 10:1 E:T ratios, respectively) and increasing concentrations of autophinib. $n = 3$ and 5 independent experiments. Error bars, s.e.m. (**a**, **b**). *P* values determined by two-way ANOVA with Fisher's LSD comparison. **c**, Rank order of 91 cancer cell lines by their sensitivity synergy score to co-treatment with recombinant TNF (ranging from 0 to 100 U ml^{-1}) and autophinib (ranging from 0 to 1,000 mM). Heat maps represent μ/μmax for all combinations in selected cell lines (MC38, A375 and NIH-2170) at 72 h after treatment. n = technical duplicates for each individual condition across all cell lines.

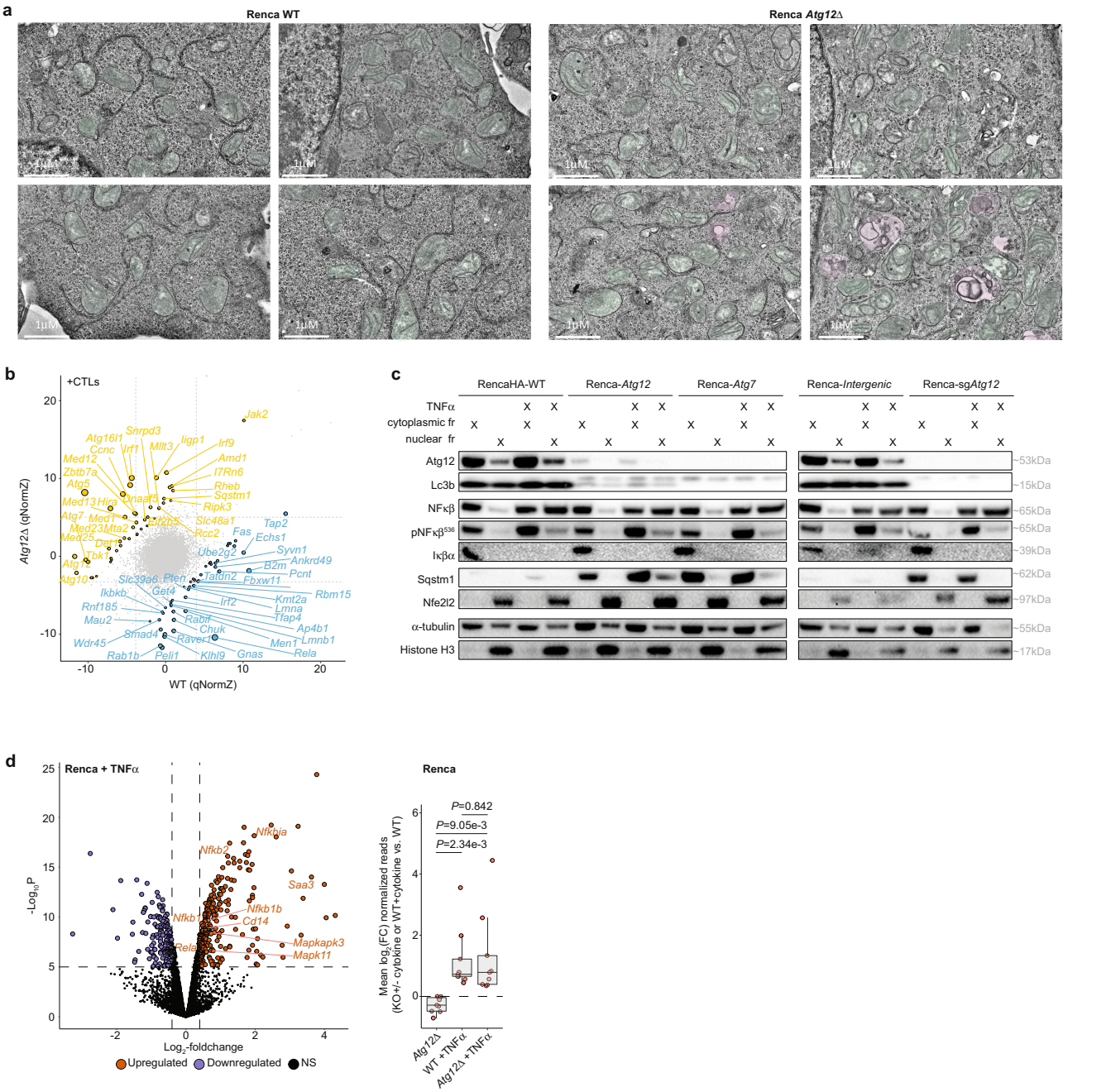

Extended Data Fig. 9 | Additional data for *Atg12*. **a**, TEM photo showing increased number of autophagosomes (purple) and mitochondria (green) in Renca *Atg12*Δ cells compared to WT cells. Data represents a single experiment. **b**, Sectored scatter plots of gene-level quantile normalized NormZ scores (qNormZ) from WT and *Atg12*Δ cells propagated under CTL selection pressure. Significant negative and positive GIs (FDR < 5%) are coloured blue and yellow, respectively. Dashed line reflects median NormZ of GIs. **c**, Western blot depicting levels of select autophagy, NF-κβ and Nrf2 pathway-associated proteins in isogenic Renca−HA WT, *Atg12*Δ or Atg7Δ cells, as well as intergenic or *Atg12* gRNA-transduced polyclonal KO Renca cell populations. Data represent a single experiment reflective of 3 independent biological replicates. **d**, Differential gene expression between TNF-treated WT and *Atg12*Δ Renca cells highlighting downregulated (purple; $n = 190$) and upregulated (orange; $n = 251$) genes (FDR < 0.05). Representative genes for the Reactome NF-κβ pathway (R-HSA-975138.1) are labelled ($n = 12$). Side box plots display mean fold change (where fold change = $\log_2$(KO or WT read counts ± cytokine) − $\log_2$(WT read counts)) of ER stress pathway genes between *Atg12*Δ, TNF-treated or *Atg12*Δ + TNF treatment conditions relative to WT cells. Boxes show the interquartile range (IQR, 25th to 75th percentile), with the median indicated by a line. The whiskers extend to the quartile ± 1.5 × IQR. Data representative of 3 independent biological replicates, and statistical significance was determined by a two-sided Student's *t*-test between each treatment condition group.

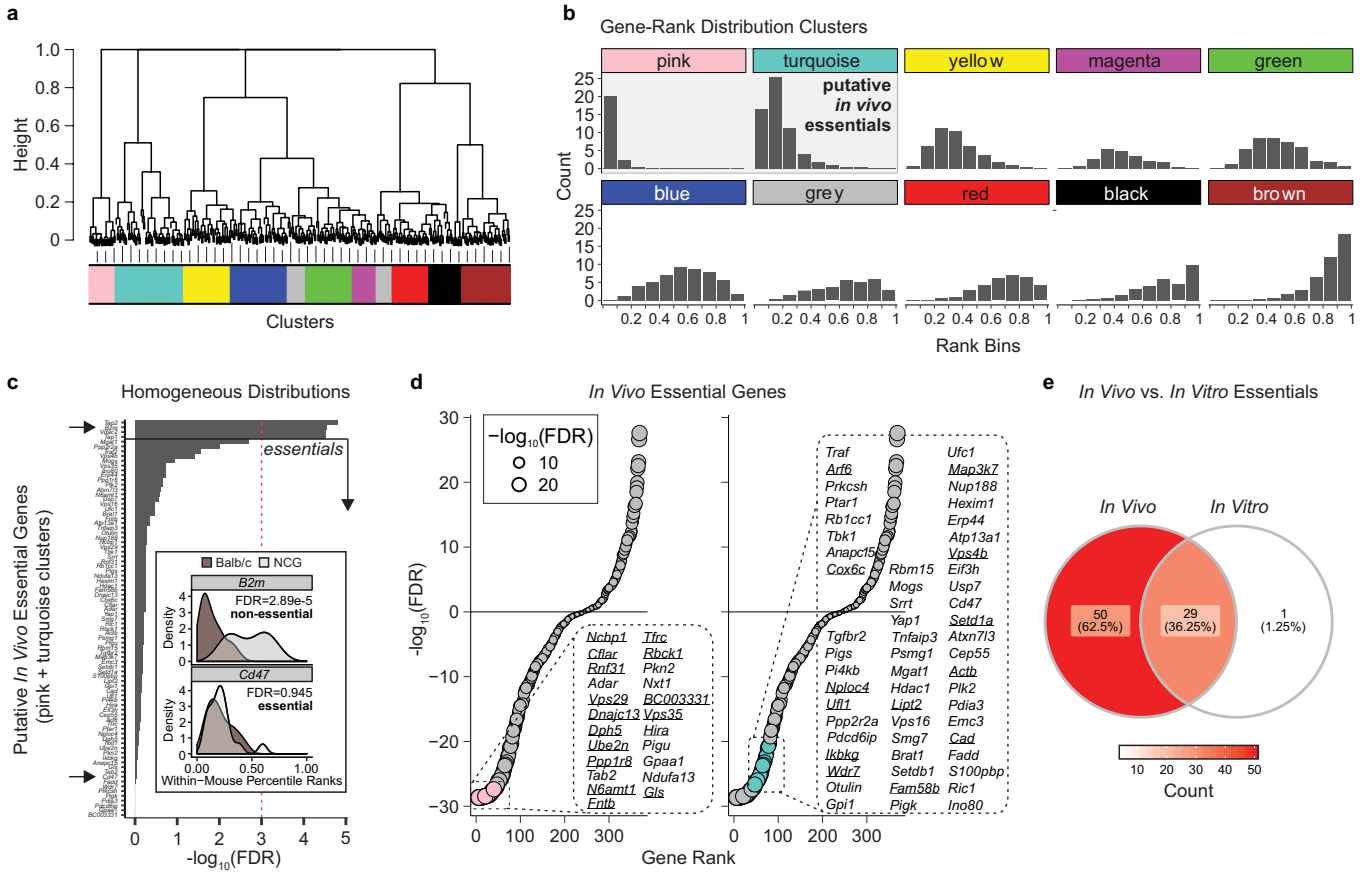

Extended Data Fig. 10 | Analysis of in vivo essential genes. a, Hierarchical clustering of gene-level rank distributions. NCG and BALB/c were pooled and only early time point data was considered. Individual genes were ranked according to normalized gRNA counts within each mouse sample, and the resulting gene-level ranks were pooled across mice and hierarchically clustered using Jensen-Shannon divergence. Clusters were defined through adaptive branch pruning. **b**, Characteristic gene-rank distributions for each cluster. Pink and turquoise clusters were classified as putative essentials. **c**, Identifying bona fide in vivo essential genes among putative in vivo essential gene clusters. Rank distributions of putative essential genes (identified in **a**, **b**) were stratified by mouse strain (brown, BALB/c; grey, NCG); strain-dependent differences were evaluated using two-sided Wilcoxon rank sum test and *P* values were Benjamini–Hochberg-adjusted. Genes were then ranked by *P* value, and genes for which rank distributions were consistent between strains (that is, FDR > 0.001) were classified as in vivo essential genes. Insets: Comparison of strain-dependent rank distributions for representative in vivo non-essential gene (*B2m*) and essential gene (*Cd47*). **d**, Rank plot of in vivo essentials stratified by pink and turquoise clusters. Underlined genes are those that were also classified as essentials in in vitro EMT6 screens. **e**, Overlap between essential genes found in in vitro and in vivo EMT6 screens. In vitro essential genes were identified at BF > 50, and in vivo essential genes were those belonging to pink and turquoise clusters shown in **a** and **b**, and exhibiting strain-independent rank distributions as shown in **c**.

nature research

Corresponding author(s): Jason Moffat

Last updated by author(s): Sep 10, 2020

Reporting Summary

Nature Research wishes to improve the reproducibility of the work that we publish. This form provides structure for consistency and transparency in reporting. For further information on Nature Research policies, see Authors & Referees and the Editorial Policy Checklist.

Statistics

For all statistical analyses, confirm that the following items are present in the figure legend, table legend, main text, or Methods section.

n/a	Confirmed	
☐	☒	The exact sample size (*n*) for each experimental group/condition, given as a discrete number and unit of measurement
☐	☒	A statement on whether measurements were taken from distinct samples or whether the same sample was measured repeatedly
☐	☒	The statistical test(s) used AND whether they are one- or two-sided *Only common tests should be described solely by name; describe more complex techniques in the Methods section.*
☒	☐	A description of all covariates tested
☐	☒	A description of any assumptions or corrections, such as tests of normality and adjustment for multiple comparisons
☐	☒	A full description of the statistical parameters including central tendency (e.g. means) or other basic estimates (e.g. regression coefficient) AND variation (e.g. standard deviation) or associated estimates of uncertainty (e.g. confidence intervals)
☐	☒	For null hypothesis testing, the test statistic (e.g. *F*, *t*, *r*) with confidence intervals, effect sizes, degrees of freedom and *P* value noted *Give P values as exact values whenever suitable.*
☐	☒	For Bayesian analysis, information on the choice of priors and Markov chain Monte Carlo settings
☐	☒	For hierarchical and complex designs, identification of the appropriate level for tests and full reporting of outcomes
☐	☒	Estimates of effect sizes (e.g. Cohen's *d*, Pearson's *r*), indicating how they were calculated

Our web collection on statistics for biologists contains articles on many of the points above.

Software and code

Policy information about availability of computer code

Data collection	Sequencing: Illumina HiSeq2500, Nextseq500, Novaseq 6000 (https://www.illumina.com/) Flow cytometry: FACSDIVA v6 Incucyte S3 system (https://www.essenbioscience.com/en/products/incucyte/incucyte-s3/) Incucyte Zoom system (https://www.essenbioscience.com/en/resources/incucyte-zoom-resources-support/)
Data analysis	Bowtie v0.12.8 - used to align and analyze reads from pooled CRISPR screen (https://en.wikipedia.org/wiki/Bowtie_(sequence_analysis)) Python v 2.7.13 and v 3.7.4, various functions DrugZ v1 (https://github.com/hart-lab/drugz) Bagel v2 (https://github.com/hart-lab/bagel) R v3.6.1: various functions, (http://cran.utstat.utoronto.ca) RStudio: v1.1.456, various functions (http://rstudio.com/products/rstudio/download/#download) GraphPad Prism v8.2.1, statistical analysis software (https://www.graphpad.com/scientific-software/prism/) Microsoft Excel v16.16.12, general table organization FlowJo™ v10.6.1 (https://www.flowjo.com/solutions/flowjo), analysis of flow cytometry data Incucyte S3 Software v2018A, analysis of in vitro cell assay data Incucyte Zoom Software v2016A, analysis of in vitro cell assay data Limma v3.40.2, for RNAseq analysis FACSDIVA v6, for flow cytometry analysis Tecnai Microscope control software v 4.0, for TEM analysis edgeR package v3.26.5 (https://bioconductor.org/packages/release/bioc/html/edgeR.html), for RNAseq analysis Cytoscape v3.7.1, for pathway analysis Enrichment map v.3.5.1 w/ autoannotate plugin v1.3, for pathway analysis gProfileR v0.6.7, for pathway analysis ggplot2 v3.2.0, for various plots/figures GSEA v3.0 (https://www.gsea-msigdb.org/gsea/index.jsp), for pathway analysis

cdgsr v1.3.0 - for analysis of TCGA data
TCGAbiolinks v2.16.0 - for analysis of TCGA data
ppcor R package v1.1 - for TCGA analysis spearman correlations

For manuscripts utilizing custom algorithms or software that are central to the research but not yet described in published literature, software must be made available to editors/reviewers. We strongly encourage code deposition in a community repository (e.g. GitHub). See the Nature Research guidelines for submitting code & software for further information.

Data

Policy information about availability of data

All manuscripts must include a data availability statement. This statement should provide the following information, where applicable:

- Accession codes, unique identifiers, or web links for publicly available datasets
- A list of figures that have associated raw data
- A description of any restrictions on data availability

All raw data has been provided in supplemental tables, source data tables or will be made available upon publication or on request. There is no restriction on data availability.
Links to publicly available datasets analyzed in this manuscript:
Bader lab pathway genesets (http://download.baderlab.org/EM_Genesets/)
g:Profiler(https://biit.cs.ut.ee/gprofiler/gost)
TCGA cBioportal (https://www.cbioportal.org/)

Data source files for raw data are provided for:
Figure 2B,
Figure 3B,C
EDF 4C,D
EDF 5B,C,E,F,G
EDF 6E
EDF 7D,E,F
EDF 8A,B,C
EDF 9C
Cell line inventory table

Field-specific reporting

Please select the one below that is the best fit for your research. If you are not sure, read the appropriate sections before making your selection.

☒ Life sciences ☐ Behavioural & social sciences ☐ Ecological, evolutionary & environmental sciences

For a reference copy of the document with all sections, see nature.com/documents/nr-reporting-summary-flat.pdf

Life sciences study design

All studies must disclose on these points even when the disclosure is negative.

Sample size	For small-scale experiments, the number of replicates exceeds at least 2 biological replicates (=independent experiments) and/or at least 3 technical replicates repeated measurements of the same original sample). For screens, the initial mutagenized cell pool was split into 3 replicates post-selection and processed independently in all downstream steps. Using these sample sizes allowed for the application of robust statistical assessments for each experiment or analysis. The sample sizes were chosen according to the convention in the field. Relevant references published previously in Nature include (PMID): 30971826, 30760928, 29995852, 29973717.
Data exclusions	No data were excluded from any experiments and figures shown. For Fig2B, replicate experiments are included in the source data files and not the figures for brevity. For Fig 3C, data from higher doses (E:T 0.6, 1.2) were included in the source data files but not the figures for brevity.
Replication	We present no experimental results that were not reproducible. Notably, the autophinib / TNFa screen done included one cell line as a control ran with every batch (H2170, in a total of 10 batches) that yielded consistent positive synergy scores.
Randomization	Randomization was performed for the Adar knockdown experiment, where mice were randomized prior to addition of doxycycline. For all other experiments randomization was not relevant as allocation of samples into experimental groups was pre-determined according to the experimental setup as described in each figure/methods section.
Blinding	No blinding was performed in the in vivo adar validation experiment as mice were provided colored food in order to facilitate dox induction making it obvious the treatment group mice. For all other experiments, blinding was not performed as samples and mice were allocated into pre-specified groups, and readouts were automated (e.g. plate reader, coulter counter, illumina sequencing). Notably, blinding is not the convention for these types of experiments across the field. Relevant references published previously in Nature include (PMID): 30971826, 30760928, 29995852, 29973717.

Reporting for specific materials, systems and methods

We require information from authors about some types of materials, experimental systems and methods used in many studies. Here, indicate whether each material, system or method listed is relevant to your study. If you are not sure if a list item applies to your research, read the appropriate section before selecting a response.

Materials & experimental systems

n/a	Involved in the study
☐	☒ Antibodies
☐	☒ Eukaryotic cell lines
☒	☐ Palaeontology
☐	☒ Animals and other organisms
☒	☐ Human research participants
☒	☐ Clinical data

Methods

n/a	Involved in the study
☒	☐ ChIP-seq
☐	☒ Flow cytometry
☒	☐ MRI-based neuroimaging

Antibodies

Antibodies used

Antibodies used for Western blots: ATG12 (20H24L24) (701684, Invitrogen, 1:250), LC3b (ab51520, Abcam, 1:3000), NF-κB p65 (D14E12) (#8242, Cell signalling, 1:1000), Phospho-NF-κB p65 (Ser536) (93H1) (#3033, Cell signalling, 1:1000), IκBα (#9242, Cell signalling, 1:1000), NRF2/NFE2L2 (D1Z9C) (#12721, Cell signalling, 1:1000), SQSTM1/P62 (#5114, Cell signalling, 1:1000), alpha tubulin (T6074, Sigma Millipore, 1:5000), Histone H3 (#9715, Cell signalling, 1:1000), Bip (C50B12, Cell signalling, 1:1000), GAPDH (2118S, Cell signalling, 1:5000). Secondary antibodies used were IRDye 680RD Donkey anti-Rabbit (926–68073, LI-COR, 1:5000) and IRDye 800CW Donkey anti-Mouse (926–32212, LI-COR, 1:5000). Antibodies used for flow cytometry: MHC-I (anti mouse MHC-I (H-2kb) EFluor450 at 1:200, clone AF6-88.5.5.3, Ebiosciences), MHC-I bound OVA (anti mouse OVA 257-264 peptide bound to H2kb PE at 1:100, clone 25-D1.16, Ebiosciences). Antibodies for cell based assays: anti-TNFa (MP6-XT22, Biolegend Cat No. 506331), anti-IFNg (XMG1.2, Biolegend Cat No. 505834).

Validation

Antibody catalog numbers are provided above for manufacturer's validation specifications. No validation beyond manufacturer's specifications were performed.
A list of vendor validated applications includes:
- ATG12 (20H24L24) (701684, Invitrogen): western blot (WB), immunocytochemistry (ICC), immunoflouresence (IF)
- LC3b (ab51520): immunohistochemistry (IHC), Flow Cytometry (FC), WB, ICC, IF
- NF-κB p65 (D14E12) (#8242, Cell signalling): WB, Immunoprecipitation (IP), IHC, Chromatin Immunoprecipitation (ChIP), IF, FC, ELISA-Peptide (EP).
- Phospho-NF-κB p65 (Ser536) (93H1) (#3033, Cell signalling): WB, IP, IF, F.
- IκBα (#9242, Cell signalling): WB, IP.
- NRF2/NFE2L2 (D1Z9C) (#12721, Cell signalling): WB, IP, ChIP, FC.
- SQSTM1/P62 (#5114, Cell signalling): WB.
- alpha tubulin (T6074, Sigma Millipore): WB, ICC, IP.
- Histone H3 (#9715, Cell signalling): WB.
- Bip (C50B12, Cell signalling): WB, IHC, FC.
- GAPDH (2118S, Cell signalling): WB, IHC, IF, FC.
- IRDye 680RD Donkey anti-Rabbit (926–68073, LI-COR): WB.
- IRDye 800CW Donkey anti-Mouse (926–32212, LI-COR): WB.
- anti mouse MHC-I (H-2kb) EFluor450 at 1:200, clone AF6-88.5.5.3, Ebiosciences: FC.
- anti mouse OVA 257-264 peptide bound to H2kb PE at 1:100, clone 25-D1.16, Ebiosciences): FC.
- anti-TNFa (MP6-XT22, Biolegend Cat No. 506331): ELISA, intracellular flow cytometry (ICFC), CyTOF, IF, IHC, Neutralization (N).
- anti-IFNg (XMG1.2, Biolegend Cat No. 505834: ELISA, ELISPOT, CyTOF, ICFC, IHC, WB, N.

Eukaryotic cell lines

Policy information about cell lines

Cell line source(s)

Cell lines were originally purchased from the following sources:

American Type Culture Collection: A375, A-431, CHL1, COLO 829, G-361, HMCB, HT-144, BxPC-3, Capan-1, Capan-2, CFPAC-1, HPAC, HPAF-II, Hs 766T, MIA, PaCa-2, PANC1, PL45, SU.86.86, KLE, A549, Calu-6, ChaGo-k-1, DMS-153, NCI-H1048, NCI-H1155, NCI-H1299, NCI-H1355, NCI-H1437, NCI-H1573, NCI-H1581, NCI-H1650, NCI-H1651, NCI-H1703, NCI-H1734, NCI-H1770, NCI-H1793, NCI-H1975, NCI-H2009, NCI-H2030, NCI-H2052, NCI-H2081, NCI-H2110, NCI-H2122, NCI-H2126, NCI-H2170, NCI-H2228, NCI-H226, NCI-H23, NCI-H2347, NCI-H2452, NCI-H28, NCI-H292, NCI-H358, NCI-H446, NCI-H520, NCI-H596, NCI-H661, NCI-H774, NCI-H82, SK-Lu-1, SW-900, COLO 205, COLO-320-HSR, HCT 116, HT-29, LoVo, SNU-C1, SW48, SW620, CAMA1, CHP212, DBTRG05MG, LN18, LN-229, M059K, U-118 MG, U-138 MG, HuTu 80, OVCAR3, SW579, A-204, A673, Hs 729, RD, SJRH30, TE, 381.T, UMUC3, HEK293T, Renca, CT26, B16F10, EMT6, 4T1.

European Collection of Authenticated Cell Cultures: COR-L23, Gp2D.

Horizon Discovery: HAP1

Kerafast: MC38

Authentication

Cell lines were authenticated via:

- STR profiling: A375, A-431, CHL1, G-361, HMCB, HT-144, CFPAC-1, HPAC, Hs 766T, MIA, PL45, SU.86.86, KLE, A549, Calu-6, ChaGo-k-1, DMS-153, NCI-H1048, NCI-H1299, NCI-H1355, NCI-H1437, NCI-H1573, NCI-H1581, NCI-H1650, NCI-H1651, NCI-H1703, NCI-H1734, NCI-H1793, NCI-H1975, NCI-H2009, NCI-H2030, NCI-H2052, NCI-H2081, NCI-H2110, NCI-H2122, NCI-H2126, NCI-H2170, NCI-H2228, NCI-H226, NCI-H23, NCI-H2347, NCI-H2452, NCI-H28, NCI-H358, NCI-H520, NCI-H774, NCI-H82, SW-900, HCT 116, HT-29, LoVo, SW620, CAMA1, DBTRG05MG, U-118 MG, U-138 MG, OVCAR3, SW579, A-204, A673, Hs 729, RD, UMUC3, HEK293T.

- RNAseq: B16F10, MC38, Renca, CT26, EMT6, 4T1

- No authentication performed: COLO 829, BxPC-3, Capan-1, Capan-2, HPAF-II, PaCa-2, PANC1, NCI-H1155, NCI-H1770, NCI-H292, NCI-H446, NCI-H596, NCI-H661, SK-Lu-1, COLO 205, COLO-320-HSR, SNU-C1, SW48, CHP212, LN18, LN-229, M059K, HuTu 80, SJRH30, TE, 381.T, HAP1.

Mycoplasma contamination

All the cell lines in this study were routinely tested and confirmed negative for mycoplasma contamination.

Commonly misidentified lines
(See ICLAC register)

U-118 MG is the only cell line used in this study that appears on the commonly misidentified list. This line was purchased from ATCC and STR verified.

Animals and other organisms

Policy information about studies involving animals; ARRIVE guidelines recommended for reporting animal research

Laboratory animals

Clone 4 (CL4) T-cell receptor transgenic mice (CBy.Cg-Thy1aTg(TcraCl4,TcrbCl4)1Shrm/ShrmJ, Stock No. 005307 from The Jackson Laboratory). Female and male mice were used age 2-12 months.

OT-1 T-cell receptor transgenic mice (C57BL/6-Tg(TcraTcrb)1100Mjb/J, Stock No. 003831 from The Jackson Laboratory). Female mice aged 3-6 months were used.

C57BL/6J mice (Stock No. 000664 from the Jackson Laboratory). Female mice aged 8-12 weeks were used.

NSG mice (NOD.Cg-Prkdc(scid)Il2rg(tm1Wjl)/SzJ, Stock No. 005557 from The Jackson Laboratory). Female aged 8-12 weeks were used.

BALB/c mice (BALB/cAnNCrl, Strain Code: 028 from Charles River Laboratories). Female mice aged 8-16 weeks were used.

NCG mice (NOD-Prkdc(em26Cd52)Il2rg(em26Cd22)/NjuCrl, Strain Code: 572 from Charles River Laboratories). Female mice aged 8-16 weeks were used.

At University of Toronto, animals were housed at approximately 22±2ºC, humidity 45% on a 14-hour light, 10-hour dark cycle. At Agios, animals were housed at approximately 70±4ºF, 30-70% humidity on a 12-hour light/dark cycle.

Wild animals

Wild animals were not used in this study.

Field-collected samples

Field-collected samples were not used in this study.

Ethics oversight

The use of animals in this study followed the guidelines of the Canadian Council on Animal Care and Ontario's Animals for Research Act and The Guide for the Care and Use of Laboratory Animals (The Guide), Cambridge Public Health Laboratory Animal Ordinances and the USDA's Animal Welfare Act. The study was approved by the University Animal Care Committee at the University of Toronto and the Institutional Animal Care and Use Committee at Agios Pharmaceuticals.

Note that full information on the approval of the study protocol must also be provided in the manuscript.

Flow Cytometry

Plots

Confirm that:

☒ The axis labels state the marker and fluorochrome used (e.g. CD4-FITC).

☒ The axis scales are clearly visible. Include numbers along axes only for bottom left plot of group (a 'group' is an analysis of identical markers).

☒ All plots are contour plots with outliers or pseudocolor plots.

☒ A numerical value for number of cells or percentage (with statistics) is provided.

Methodology

Sample preparation

For the analysis of MHC-I and MHC-I bound OVA on B16-Ova, cells were treated (or not) with 10nM of mouse recombinant IFNg

Sample preparation	(78021.2, StemCell) for 96h, lifted from the culture plates using trypsin EDTA and washed once in FACS buffer (PBS containing 5% FBS). After washed, cells were stained at 4˚C for 30min in FACS buffer containing MHC-I (anti mouse MHC-I (H-2kb) EFluor450 at 1:200, clone AF6-88.5.5.3, Ebiosciences) and MHC-I bond OVA (anti mouse OVA 257-264 peptide bound to H2kb PE at 1:100, clone 25-D1.16, Ebiosciences) antibodies. After staining, cells were washed in FACS buffer, and resuspended in FACS buffer containing 1:500 of ToPro-3 for live/dead discrimination (T3606, Invitrogen).
Instrument	LSR II: 3 laser (488/640/405) configuration (BD Biosciences); LSR Fortessa X-20: 5 laser configuration (BD Biosciences)
Software	FACSDIVA v6, FlowJo v10.6.1
Cell population abundance	1:500 of ToPro-3 for live/dead discrimination (T3606, Invitrogen).
Gating strategy	Forward scatter area vs. side scatter area or height plot with gate 1 to separate cell events from debris. Forward scatter height vs. forward scatter width or area with gate 2 to separate single cells from aggregates. Forward scatter area vs. ToPro-3 with gate 3 to separate viable from dead cells. MHC-I (pacific blue-A) and MHC-I-OVA (PE-A) positive cells detected in live cells with negative gates set based on unstained controlled.

☒ Tick this box to confirm that a figure exemplifying the gating strategy is provided in the Supplementary Information.